Bora, S., Scherbaum, F., Kuehn, N., Stafford, P. (2016): On the Relationship between Fourier and Response Spectra: Implications for the Adjustment of Empirical Ground-Motion Prediction Equations (GMPEs). - *Bulletin of the Seismological Society of America*, *106*, 3, pp. 1235—1253.

DOI: http://doi.org/10.1785/0120150129

THE SEISMOLOGICAL SOCIETY OF AMERICA
400 Evelyn Ave., Suite 201
Albany, CA 94706-1375
(510) 525-5474; FAX (510) 525-7204
www.seismosoc.org

Bulletin of the Seismological Society of America, Vol. 106, No. 3, pp. 1235–1253, June 2016, doi: 10.1785/0120150129

On the Relationship between Fourier and Response Spectra: Implications for the Adjustment of Empirical Ground-Motion Prediction Equations (GMPEs)

by Sanjay Singh Bora, Frank Scherbaum,* Nicolas Kuehn, and Peter Stafford

Abstract The functional form of empirical response spectral ground-motion prediction equations (GMPEs) is often derived using concepts borrowed from Fourier spectral modeling of ground motion. As these GMPEs are subsequently calibrated with empirical observations, this may not appear to pose any major problems in the prediction of ground motion for a particular earthquake scenario. However, the assumption that Fourier spectral concepts persist for response spectra can lead to undesirable consequences when it comes to the adjustment of response spectral GMPEs to represent conditions not covered in the original empirical data set. In this context, a couple of important questions arise, for example, what are the distinctions and/or similarities between Fourier and response spectra of ground motions? And, if they are different, then what is the mechanism responsible for such differences and how do adjustments that are made to Fourier amplitude spectrum (FAS) manifest in response spectra? The present article explores the relationship between the Fourier and response spectrum of ground motion by using random vibration theory (RVT). With a simple Brune (1970, 1971) source model, RVT-generated acceleration spectra for a fixed magnitude and distance scenario are used. The RVT analyses reveal that the scaling of low oscillator-frequency response spectral ordinates can be treated as being equivalent to the scaling of the corresponding Fourier spectral ordinates. However, the high oscillator-frequency response spectral ordinates are controlled by a rather wide band of Fourier spectral ordinates. In fact, the peak ground acceleration, counter to the popular perception that it is a reflection of the high-frequency characteristics of ground motion, is controlled by the entire Fourier spectrum of ground motion. Additionally, this article demonstrates how an adjustment made to FAS is similar or different to the same adjustment made to response spectral ordinates. For this purpose, two cases: adjustments to the stress parameter ($\Delta\sigma$) (source term), and adjustments to the attributes reflecting site response (V_S–κ_0) are considered.

Introduction

In the current practice of probabilistic seismic-hazard analysis (PSHA) the most commonly used ground-motion intensity measure (GMIM) is the response spectral ordinate corresponding to a single-degree-of-freedom (SDOF) oscillator with a particular level of damping (e.g., 5% of critical damping). Consequently, most of the empirical ground-motion prediction equations (GMPEs) found in the literature are derived for response spectral ordinates of the SDOF oscillator and essentially provide an estimate of the conditional distribution of a GMIM for a particular earthquake scenario. The functional forms that are used in the development of the response spectral GMPEs are frequently based on concepts and scaling laws borrowed from Fourier spectral representations of ground motion. This transfer of concepts from a linear system domain to a nonlinear system domain may not have major consequences regarding the model predictions in a normal usage case, but in the context of the adjustment of median predictions to account for differences in seismological characteristics it can lead to some unrealistic behaviors of response spectral GMPEs. For example, the stress parameter ($\Delta\sigma$) is associated with the high-frequency signal strength in the Fourier amplitude spectrum (FAS) of ground motion (Atkinson and Beresnev, 1997) and determines the shape of the source spectrum (Brune, 1970, 1971). Similarly, the site-related attenuation parameter κ_0 is linked with the fall-off of

*On leave from Institute of Earth and Environmental Science, University of Potsdam, Germany.

high-frequency amplitudes in the FAS of accelerograms. However, as we will illustrate in this article from different perspectives, the high-frequency spectral content of response spectra is not directly proportional to the high-frequency spectral content of the corresponding Fourier spectrum. As a consequence, the stress parameter $\Delta\sigma$ and site-related attenuation parameter κ_0 influence the high-frequency content of the response spectrum in ways which might be considered counterintuitive if one simply assumes similar behavior of Fourier and response spectra.

Commonly, empirical GMPEs are derived by performing regression analysis over a database of earthquake records that are recorded at different sites. For performing a site-specific PSHA, for example, in conjunction with the single-station sigma framework (Atkinson, 2006; Rodriguez-Marek *et al.*, 2014), such GMPEs need to be adjusted to be applicable for the reference site condition to define the input motions for a site-specific site response analysis. Such adjustments made to GMPEs are called host to target adjustments; a popular framework in this context is the hybrid-empirical approach (Campbell, 2003). The term "host" refers to the data-rich region for which an original GMPE was derived and "target" corresponds to the site/region for which the PSHA is to be undertaken. In the hybrid-empirical approach the ratios of stochastically simulated (Boore, 1983, 2003) response spectral ordinates, that is, target response spectra/host response spectra, are usually applied to the existing GMPEs (from the data-rich host regions) to account for the regional differences in the underlying seismological parameters. Such adjustments are based upon the assumption that the regional differences that exist between the FAS of the ground motion for the host and target are all and well captured by the corresponding ratio of response spectral ordinates. However, this may not be true over the entire range of oscillator frequencies (or periods) as shown later in this article.

In an attempt to bridge the gap between common engineering practices and seismological understanding, the present article is aimed at providing some guidance regarding the relationship between the FAS and the response spectrum of ground motion. The relationship between the two will be discussed for response spectral ordinates of acceleration corresponding to a 5% damped SDOF oscillator. That is followed by discussing the implications of this relationship for the adjustment of response spectral GMPEs. We make use of random vibration theory (RVT) to represent the response spectrum in terms of the Fourier spectrum of ground motion. The seminal work of Hanks and McGuire (1981) first used RVT in engineering seismology to predict the peak ground acceleration (PGA) through the use of the FAS of ground motion. Boore (1983, 2003) extended this theory to the stochastic simulation method, an extensively used tool worldwide for synthesizing ground motions for engineering applications. This simulation method is based upon the inherent assumption that the high-frequency ground motions of engineering interest are characterized by having a randomly distributed phase spectrum and an amplitude spectrum that is defined by a simple analytical Fourier spectral model which accounts for geometrical spreading, inelastic (Q) and κ_0 related attenuation with respect to Brune's source spectrum (among other possible source spectra). The details of RVT, as far as the present article is concerned, and the important equations involved in the context of ground-motion simulation are discussed in the following section. This is followed by other relevant applications and validations of RVT in engineering seismology and seismic-hazard studies. Subsequently, we break the response spectrum obtained by RVT into its constituent elements that we refer to as the "Building blocks of the response spectrum". We will use this concept to describe the characteristics of the FAS of ground motion that influence the response spectrum at a particular oscillator frequency. Finally, the implications of the relationship between the FAS and the response spectrum are discussed in the context of host-to-target adjustments in terms of source parameters, such as $\Delta\sigma$, and attributes of the local site conditions, such as κ_0 and the shear-wave velocity (V_S) profile.

Response Spectra from an RVT Perspective

The key feature of the RVT framework is that it relates the peak value of the time-domain motion to the FAS representation of the motion and its duration through Parseval's theorem and extreme value statistics. The first use of RVT in engineering seismology goes back to the work of Hanks and McGuire (1981) to predict the PGA from the root mean square (rms) acceleration y_{rms}. Parseval's theorem is used to compute y_{rms} from the FAS, $|Y_{\text{gm}}(f)|$, of the ground-motion. Hanks and McGuire (1981) related PGA to y_{rms} using a peak factor (PF) of Vanmarcke and Lai (1980), which is a function of duration along with a measure of the predominant frequency of the ground motion in question.

Boore (1983, 2003) extended this approach of computing PGA from the FAS of ground motion to the computation of response spectral ordinates of an SDOF system in his stochastic simulation method using a simple analytical model for the FAS of ground motion. Boore used the PF of Cartwright and Longuet-Higgins (1956) to relate the response spectral ordinate y_{max} of the SDOF oscillator corresponding to the damping ratio ζ at an oscillator frequency f_{osc} with the y_{rms} given as follows:

$$\frac{y_{\text{max}}(f_{\text{osc}},\zeta)}{y_{\text{rms}}(f_{\text{osc}},\zeta)} = \sqrt{2}\int_0^\infty \{1-[1-\xi\exp(-z^2)]^{N_e}\}\mathrm{d}z, \quad (1)$$

in which the variable of integration z is a random variable related to the ratio of the maximum to rms value in a stationary process with N_e extrema. The expression in equation (1) is referred to as the PF, and within this expression,

$$\xi(f_{\text{osc}},\zeta) = \frac{m_2(f_{\text{osc}},\zeta)}{\sqrt{m_0(f_{\text{osc}},\zeta)m_4(f_{\text{osc}},\zeta)}}, \quad (2)$$

is a measure of the bandwidth of the motion, and the number of extrema N_e is given by

$$N_e(f_{osc},\zeta) = \frac{1}{\pi}\sqrt{\frac{m_4(f_{osc},\zeta)}{m_2(f_{osc},\zeta)}}D_{gm}. \quad (3)$$

Here, D_{gm} is the duration of the ground motion (Boore, 2003), which is assumed to be the sum of a source duration (related to the inverse of Brune's corner frequency) and a path-dependent duration. In equation (3), m_0, m_2, and m_4 are the spectral moments of the oscillator response as defined in equation (4). It is to be noted that in this context y_{max} and y_{rms} are computed as functions of oscillator frequency f_{osc}. This is different from the original formulation of Hanks and McGuire (1981) and Vanmarcke and Lai (1980), who used observed FAS, $|Y_{gm}(f)|$, values of the ground motion directly to compute PGA. Therefore, in the computation of spectral moments, that is, m_k, in which $k = 0, 2, 4$, the squared FAS of the SDOF response, $|Y_{SDOF}(f, f_{osc}, \zeta)|^2$ is used as follows:

$$m_k(f_{osc},\zeta) = 2\int_0^\infty (2\pi f)^k |Y_{SDOF}(f, f_{osc}, \zeta)|^2 df. \quad (4)$$

In the above equation, $|Y_{SDOF}(f, f_{osc}, \zeta)|^2$ is obtained by multiplying $|Y_{gm}(f)|^2$ with the squared SDOF transfer function $|I(f, f_{osc}, \zeta)|^2$ as

$$|Y_{SDOF}(f, f_{osc}, \zeta)|^2 = |Y_{gm}(f)|^2 |I(f, f_{osc}\zeta)|^2 \ldots, \quad (5)$$

in which the SDOF transfer function $|I(f, f_{osc}, \zeta)|$ is defined as in equation (6):

$$|I(f, f_{osc}, \zeta)| = \frac{f_{osc}^2}{\sqrt{(f^2 - f_{osc}^2)^2 + (2f f_{osc}\zeta)^2}}. \quad (6)$$

The y_{rms} in equation (1) is computed as

$$y_{rms}(f_{osc},\zeta) = \left(\frac{m_0(f_{osc},\zeta)}{D_{rms}}\right)^{1/2}. \quad (7)$$

D_{rms} is the rms duration that differs from the ground-motion duration D_{gm} according to the relationship described in equation (8). As already noted by Boore (2003), earthquake records cannot be considered stationary in the strict sense and the response of the resonant systems (e.g., local soil layering or the SDOF oscillators) to those motions might include significant correlations between adjacent peaks. That means that both of these characteristics discussed in the previous sentence violate basic assumptions of the RVT framework discussed above. Notwithstanding this, Boore (2003) and some other studies (such as Hanks and McGuire, 1981; Boore, 1983; Atkinson, 1984; Rathje and Ozbey, 2006) have shown that RVT-based simulations of ground motion can capture most of the characteristics of ground motions of engineering interest. Based upon numerical experiments, Boore and Joyner (1984), Liu and Pezeshk (1999), Boore (2003), and recently Boore and Thompson (2012) suggested modifications to the duration model for the computation of the y_{rms} motion, to apply this theory to the response motion of an SDOF system. Therefore, a different measure of duration D_{rms} is used in equation (7) to compute the y_{rms} using the Boore and Thompson (2012) model to relate D_{rms} to D_{gm} as in the following:

$$\frac{D_{rms}}{D_{gm}} = \left(c_1 + c_2\frac{1-\eta^{c_3}}{1+\eta^{c_3}}\right)\left\{1 + \frac{c_4}{2\pi\zeta}\left(\frac{\eta}{1+c_5\eta^{c_6}}\right)^{c_7}\right\}. \quad (8)$$

Here, $\eta = D_0/D_{gm}$, and $D_0 = 1/(2\pi f_{osc}\zeta)$ is regarded as the oscillator duration (Boore, 2003; Boore and Thompson, 2012). Using simulated D_{rms}/D_{gm} ratios, Boore and Thompson (2012) suggest a set of regression coefficients, c_1–c_7 (in equation 8) for each magnitude–distance pair in the 4–8 magnitude range at logarithmically spaced distances from 2 to 1262 km.

Validation of the RVT Method Seen in Previous Studies

There has been a significant number of applications of RVT in engineering seismology and in studies related to seismic-hazard analysis. Pioneering efforts in this context are those of McGuire and Hanks (1980), Hanks and McGuire (1981), and McGuire *et al.* (1984). Hanks and McGuire (1981) demonstrated that bandlimited white Gaussian noise can be used to approximate, to a certain extent, the rms and peak acceleration of 300 ground-acceleration records from 16 California earthquakes. The first validation of the RVT method was done by McGuire *et al.* (1984) in which they demonstrated that the RVT simulated spectral velocities agreed well with the recorded data of the 1971 San Fernando earthquake of magnitude M_w 6.6. Regardless of the fact that earthquake ground motions cannot be considered as purely stochastic, the work of Hanks and McGuire (1981) can be considered a landmark, because it demonstrated that a seismological source model can be coupled with RVT to obtain the peak values of earthquake ground motion.

Boore (1983, 2003) extended and modified this approach to predict response spectral ordinates of an SDOF system subjected to earthquake ground motion as input. In his stochastic simulation method, Boore compared the predictions from the RVT method with those from time-domain simulations. The time-domain simulations were based on the assumptions that the engineering notion of ground motion is essentially related to the high frequencies of a ground-motion spectrum and hence warrants the use of random phase angles in conjunction with a deterministic FAS for the ground motion. Boore showed that the response spectral ordinates predicted by the RVT method agreed well with the average values of time-domain simulations, although a large number of time-domain simulations are needed before stable statistics can be computed from the time-domain maxima.

In addition, RVT has been used as an alternative approach to time-domain site-response analysis (e.g., Schneider *et al.*, 1991; Stepp *et al.*, 1991; Silva *et al.*, 1997; Rathje and Ozbey, 2006). The RVT-based site response analysis is essentially an extension

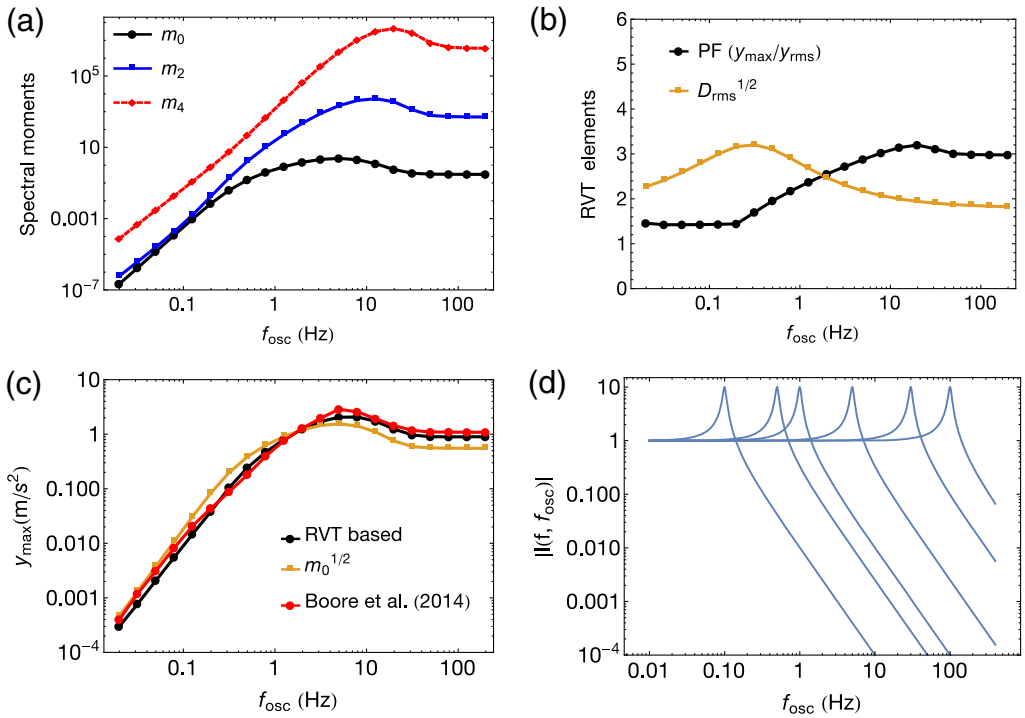

Figure 1. Building blocks of the response spectrum, y_{max} as used in random vibration theory (RVT). The stochastic model parameters for western North America (table 2 in Campbell, 2003) are used for the simulations. (a) Variation of three spectral moments m_0, m_2, and m_4 against oscillator frequency (f_{osc}). (b) The same variation of the selected peak factor and $D_{rms}^{1/2}(f_{osc})$. (c) The final response spectrum, $y_{max}(f_{osc})$ computed using RVT (black curve), response spectrum obtained by Boore *et al.* (2014) model and $m_0^{1/2}$. (d) Single degree of freedom (SDOF) oscillator transfer function $|I(f, f_{osc})|$ at different oscillator frequencies. The simulations are shown for the scenario earthquake of M_w 6 at $R_{JB} = 20$ km. The color version of this figure is available only in the electronic edition.

of the stochastic ground-motion simulation method developed to predict PGA and response spectral ordinates. Essentially, in the RVT-based site response analysis the FAS at the base of the soil column (or the rock FAS) is modified to account for the soil response to obtain the response spectral ordinates at the ground surface using RVT.

The Building Blocks of Response Spectra

To better understand the relationship between the Fourier and response spectrum within the RVT framework, we break the RVT obtained response spectrum into what we call its building blocks. Judging from equations (1–8), these are the spectral moments, the PF, that is, y_{max}/y_{rms} (equation 1) and the duration D_{gm}. It is evident from equation (1) that y_{max} is PF times the value of y_{rms} and from equation (7) that y_{rms} depends upon the zeroth-spectral moment m_0 and D_{rms}. However, D_{rms} is also a function of D_{gm} as can be seen from equation (8) and so we can refer to the oscillator-frequency independent D_{gm} as being one of the building blocks. It is worth emphasizing again that the computation of $y_{max}(f_{osc}, \zeta)$ utilizes the squared FAS of the SDOF oscillator, that is, $|Y_{SDOF}(f, f_{osc}, \zeta)|^2$ to compute the spectral moments. Given that the present analysis discusses the case of 5% damped ($\zeta = 0.05$) SDOF oscillator, a simple notation of $|I(f, f_{osc})|$ will be used for $|I(f, f_{osc}, \zeta)|$, unless a different value of ζ is used. The same notation scheme shall apply to other elements which are derived using $|I(f, f_{osc}, \zeta)|$. Additionally, throughout the following discussion our focus will be upon the relationship between acceleration response spectra and the FAS of acceleration.

Figure 1 depicts the response spectrum and the constituent spectral moments as well as the PF for a scenario earthquake of M_w 6 at distance $R_{JB} = 20$ km. The simulations are performed at an equivalent rupture distance $R_{rup} = 23$ km obtained by converting R_{JB} using the distance conversion relation suggested by Scherbaum *et al.* (2004). Although the FAS is normally prescribed in terms of the point-source metric hypocentral distance, we use the rupture distance here to approximate the effects of finite rupture. For computing the FAS, that is, the $|Y_{gm}(f)|$, stochastic model parameters for western North America (WNA) suggested by Campbell (2003) are used. Figure 1a shows the variation of the three spectral moments (m_0, m_2, and m_4) with oscillator frequency f_{osc}; in Figure 1b the variation of the PF and $D_{rms}^{1/2}$ with f_{osc} is depicted. Figure 1c shows the response spectra (i.e., y_{max} in equation 1). The $m_0^{1/2}(f_{osc})$ is included in Figure 1c to permit the reader to appreciate the similarity between $m_0^{1/2}(f_{osc})$ and the response spectrum. In the same figure, the gray curve depicts the response spectrum obtained from the empirical model of Boore *et al.* (2014). The SDOF oscillator transfer

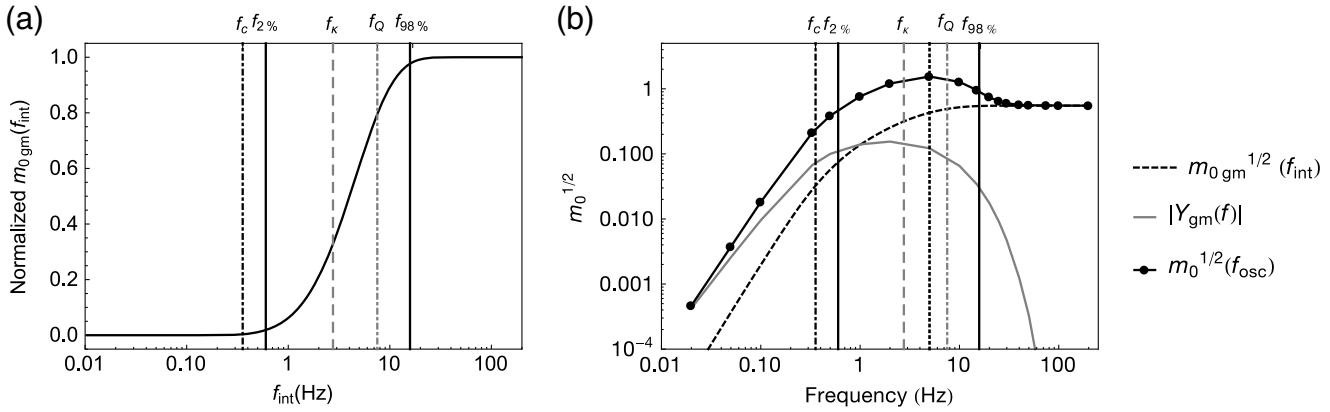

Figure 2. Plot depicting the contribution of Fourier spectral amplitudes, $|Y_{gm}(f)|$ to the response spectral amplitudes at low and high oscillator frequencies. (a) Normalized zeroth-spectral moment m_{0gm} as a function of frequency, f_{int} that is computed as described in equation (9) using $|Y_{gm}(f)|^2$. The vertical lines correspond to the source-corner frequency, f_c, $f_{2\%}$, half-power points related f_κ and f_Q, and $f_{98\%}$. (b) The square root of zeroth-spectral moment $m_0^{1/2}(f_{osc})$ (thick solid black curve) is considered to represent all the chracterstics of the response spectrum $y_{max}(f_{osc})$ (see Fig. 1c). The gray curve represents $|Y_{gm}(f)|$ corresponding to the input Fourier amplitude spectrum (FAS) (without the SDOF response); and the dashed curve indicates the (square root of) integral of $|Y_{gm}(f)|^2$, that is, $m_{0gm}^{1/2}(f_{int})$. The plots are shown for magnitude M_w 6 at a distance $R_{JB} = 20$ km; and the same stochastic model parameters as used for Figure 1.

function (equation 6) is shown in Figure 1d. It can be readily observed from Figure 1c that all the characteristics (in terms of shape and values) of the response spectrum, that is, $y_{max}(f_{osc})$ are well captured in $m_0^{1/2}(f_{osc})$. This similarity of shapes between $y_{max}(f_{osc})$ and $m_0^{1/2}(f_{osc})$ becomes more clear if one rearranges the terms in equation (1) and (7) to obtain $y_{max} = \mathrm{PF}(m_0/D_{rms})^{1/2}$. Figure 1b indicates that PF and $D_{rms}^{1/2}$ are observed to show less variation with f_{osc} as compared to $m_0^{1/2}(f_{osc})$ (keeping in mind the moment is shown using a logarithmic ordinate). In other words, the dynamic range (ratio of maximum-to-minimum) of $m_0^{1/2}(f_{osc})$ in comparison to that of PF and $D_{rms}^{1/2}$ is larger and closer to the dynamic range of the $y_{max}(f_{osc})$. This similarity facilitates one to use $m_0^{1/2}(f_{osc})$ as a proxy for the corresponding $y_{max}(f_{osc})$ to understand the behavior of the latter in terms of the FAS of ground motion $|Y_{gm}(f)|$. Therefore, in what follows $m_0^{1/2}(f_{osc})$ will be used interchangeably for $y_{max}(f_{osc})$ (for the case of $\zeta = 0.05$) to relate it with the $|Y_{gm}(f)|$ of ground motion.

Before proceeding further, we would like to emphasize that in investigating the relationship between the FAS and response spectrum of an SDOF oscillator it is important to keep in mind the difference between the oscillator frequency represented by f_{osc} and the signal frequency of the harmonic components of the Fourier spectrum denoted by f. In addition, the distinct difference between the FAS of the ground-motion $|Y_{gm}(f)|$ and that of SDOF response $|Y_{SDOF}(f, f_{osc})|$ should also be noted. The similarity between $m_0^{1/2}(f_{osc})$ and $y_{max}(f_{osc})$ exhibited in Figure 1 makes $m_0^{1/2}(f_{osc})$ a useful quantity to understand the relationship between FAS and response spectrum of ground motion. Not only that, and as will be shown in the following discussion, the zeroth-spectral moment of an acceleration response signal is also a measure of the total power of acceleration per unit mass contained in the response signal. Therefore, it is useful to note the difference in the three different measures of zeroth-spectral moment (m_0), which will be computed herein for the present analysis. As can be appreciated from equation (4), m_0 is computed as an integration of $|Y_{SDOF}(f, f_{osc}, \zeta)|^2$ over the full frequency range (f from 0 to infinity) leaving it a function of f_{osc} and ζ, that is, $m_0(f_{osc}, \zeta)$. For a fixed f_{osc} and ζ (0.05 in this study), a portion of m_0 can also be computed as a function of f_{int}, that is, $m_0(f_{int}, f_{osc})$ in which f_{int} is the upper limit of Fourier frequency used in the integration in equation (4). The notion of power "per unit mass" makes strict sense when referring to these moments obtained from the oscillator response. However, we will also refer to power more generally hereafter for moments computed from other signals. As shown in Figure 2a, $m_{0gm}(f_{int})$ can be computed using the m_0-kernel function $|Y_{gm}(f)|^2$ corresponding to the FAS of the ground motion without the oscillator transfer function as

$$m_{0gm}(f_{int}) = 2\int_0^{f_{int}} |Y_{gm}(f)|^2 \mathrm{d}f. \qquad (9)$$

The $m_{0gm}(f_{int})$ can be regarded as representing the accumulation of power (of acceleration) as a function of frequency in the spectrum in which $m_{0gm}(f_{int})$ computed at f_{int} = Nyquist frequency of the signal, represents the total power contained in the signal. The important difference to be noted hereafter is that the $m_0(f_{osc})$ and $m_0(f_{int}, f_{osc})$ use the m_0 kernel $|Y_{SDOF}(f, f_{osc})|^2$ in their computation as described in equation (4), whereas $m_{0gm}(f_{int})$ uses the $|Y_{gm}(f)|^2$ as its kernel (see equation 9). However, $m_{0gm}(f_{int})$ and $m_0(f_{int}, f_{osc})$ are

conceptually connected by the fact that they are both related to the building up of the integration in (9) and (4) as a function of f_{int} (upper frequency limit used in the integration), albeit for the two different integrands, $|Y_{\text{gm}}(f)|^2$ and $|Y_{\text{SDOF}}(f, f_{\text{osc}})|^2$, respectively. This property of $m_0(f_{\text{int}}, f_{\text{osc}})$ will be used later to indicate the dominant frequencies in $|Y_{\text{SDOF}}(f, f_{\text{osc}})|^2$ that control the final $m_0^{1/2}(f_{\text{osc}})$ at a particular oscillator frequency. Two of the three measures of the square root of the zeroth-spectral moment just discussed are plotted in Figure 2b that includes $m_0^{1/2}(f_{\text{osc}})$ as a function of f_{osc} and $m_{0\text{gm}}^{1/2}(f_{\text{int}})$ as a function of f_{int} along with the square root of the m_0 kernel ($|Y_{\text{gm}}(f)|$) corresponding to the FAS of the ground motion. Figure 2a shows normalized $m_{0\text{gm}}(f_{\text{int}})$ computed for input FAS using $|Y_{\text{gm}}(f)|^2$. It is worth noting here again, as can also be appreciated from Figure 2b, that of the two measures of $m_0^{1/2}$ it is the $m_0^{1/2}(f_{\text{osc}})$ that mimics the shape of a response spectrum.

To facilitate a relative comparison between the FAS and the response spectrum in terms of different frequency ranges, we make use of certain frequency definitions. For example, Brune's source-corner frequency f_c which is often defined to characterize the low-frequency part of the observed FAS of the ground motion (Brune, 1970). Similarly, we define the corner frequencies f_{Q} and f_κ associated with the inelastic attenuation (Q) and the high-frequency attenuation (κ_0), respectively. The f_{Q} and f_κ correspond to the frequencies at which the squared response of the corresponding filters becomes 0.5. Thus, by solving for those frequencies when assuming typical functional representations of these filters within an FAS, the analytical expressions come out to be $f_{\text{Q}} = (Q_0 \beta \ln 2/2\pi R)^{[1/(1-\alpha)]}$ and $f_\kappa = \ln 2/2\pi\kappa_0$ for f_{Q} and f_κ, respectively. Here, β is the average shear-wave velocity and α is the exponent related with the frequency-dependent quality factor.

In addition, as shown in Figure 2a, two more frequencies denoted by $f_{2\%}$ and $f_{98\%}$ indicating the frequencies corresponding to the accumulation of 2% and 98% of the final $m_{0\text{gm}}(f_{\text{int}})$ are defined. The selection of 2% and 98% level is subjective and primarily motivated by a similar definition of significant duration (in the time domain) as the time interval between two selected levels of total Arias intensity (Arias, 1970). Moreover, from Parseval's theorem, the frequencies $f_{2\%}$ and $f_{98\%}$ define a frequency range over which 96% of the total Arias intensity is encapsulated. For the scenario shown in Figure 2, the values of f_c, f_{Q}, f_κ, $f_{2\%}$, and $f_{98\%}$ are 0.36, 7.5, 2.8, 0.61, and 15.8 Hz, respectively. Essentially, these aforementioned frequencies partition the $m_0^{1/2}(f_{\text{osc}})$, and similarly the response spectrum $y_{\max}(f_{\text{osc}})$, into three different portions (Fig. 2b), one for which $f_{\text{osc}} < f_c$ or $f_{2\%}$ where the $m_0^{1/2}(f_{\text{osc}})$ decreases almost linearly with decreasing oscillator frequency, second the bell-shaped curve for which $f_{98\%} > f_{\text{osc}} > f_c$ or $f_{2\%}$ where $m_0^{1/2}(f_{\text{osc}})$ increases as function of f_{osc} and reaches a maximum (the dotted line between f_κ and f_{Q}), and third the region where it again decreases (from the maximum) with f_{osc} and finally becomes stable (the plateau) at $f_{\text{osc}} > f_{98\%}$. Therefore, the remainder of this section and Figures 2, 3, and 4 will be focused on examining what makes $m_0^{1/2}(f_{\text{osc}})$, and hence $y_{\max}(f_{\text{osc}})$, behave in this manner over these three distinct oscillator-frequency ranges.

We proceed to investigate the behavior of $m_0^{1/2}(f_{\text{osc}})$ from the high oscillator frequency, f_{osc} side of the response spectrum; the reason for this choice will become evident in the following discussion, namely that $m_0^{1/2}(f_{\text{osc}})$ at high oscillator frequencies is related to the integral of the squared spectrum of ground motion, that is, $|Y_{\text{gm}}(f)|^2$. Figure 2b depicts the contribution of $|Y_{\text{gm}}(f)|^2$ to the computation of $m_0^{1/2}(f_{\text{osc}})$. The dashed curve in Figure 2b depicts the total signal strength, represented by $m_{0\text{gm}}^{1/2}(f_{\text{int}})$, contained in the input signal distributed in a frequency range from 0 to f_{int}. When f_{int} becomes equal to the Nyquist frequency, the $m_{0\text{gm}}^{1/2}(f_{\text{int}})$ will represent square root of the total power contained in the signal. Hence, it can be easily observed from Figure 2b that the $m_0^{1/2}(f_{\text{osc}})$ at high oscillator frequencies, that is, $f_{\text{osc}} > f_{98\%}$ (the plateau) matches with the $m_{0\text{gm}}^{1/2}(f_{\text{int}})$. This implies that the oscillator action $|I(f, f_{\text{osc}})|^2$ has a minimal effect on the $y_{\max}(f_{\text{osc}})$ at those f_{osc}; in fact it is related to the total signal power (integration over the $|Y_{\text{gm}}(f)|^2$) contained in the input ground motion. This observation is further illustrated in Figure 3 and also in Figure 4. Figure 3 depicts the m_0-kernel functions $|Y_{\text{gm}}(f)|^2$ and $|Y_{\text{SDOF}}(f, f_{\text{osc}})|^2$ for the input ground motion (dashed curve) and the SDOF response (shaded curve), respectively. The shaded curve in Figure 3 represents the area spanned by $|Y_{\text{SDOF}}(f, f_{\text{osc}})|^2$ (i.e., $|Y_{\text{gm}}(f)|^2 |I(f, f_{\text{osc}})|^2$), which is effectively being used by the integral in equation (4) to compute the $m_0(f_{\text{osc}})$ at a particular oscillator frequency f_{osc}. Figure 4 depicts the effect of the SDOF oscillator $|I(f, f_{\text{osc}})|$ within $m_0^{1/2}(f_{\text{osc}})$ at low (Fig. 4a) and high (Fig. 4b) oscillator frequencies (plotted using logarithmic ordinates). As can be observed in Figure 4a, at oscillator frequencies $f_{\text{Q}} > f_{\text{osc}} \geq f_{2\%}$ mainly the peaky part (i.e., at $f = f_{\text{osc}}$) (square root) of the moment kernel $|Y_{\text{SDOF}}(f, f_{\text{osc}})|$ is controlling the $m_0^{1/2}(f_{\text{osc}})$ at a given oscillator frequency. Moreover, at oscillator frequencies lower than $f_{2\%}$, frequencies other than f_{osc} also contribute to $m_0^{1/2}(f_{\text{osc}})$, but with rapidly decaying amplitudes because $|I(f, f_{\text{osc}})|$ filters frequencies beyond f_{osc} significantly. On the other hand, at high oscillator frequencies $f_{\text{osc}} > f_{\text{Q}}$ a wide band $|Y_{\text{SDOF}}(f, f_{\text{osc}})|$, that ultimately mimics the shape of $|Y_{\text{gm}}(f)|$ at very high oscillator frequencies controls $m_0^{1/2}(f_{\text{osc}})$ (Fig. 4b). Observations from Figures 3 and 4 can be summarized in the three following points corresponding to the three different oscillator-frequency ranges.

1. At high oscillator frequencies (panels corresponding to $f_{\text{osc}} \geq 20$ Hz in Fig. 3), with increasing oscillator fre-

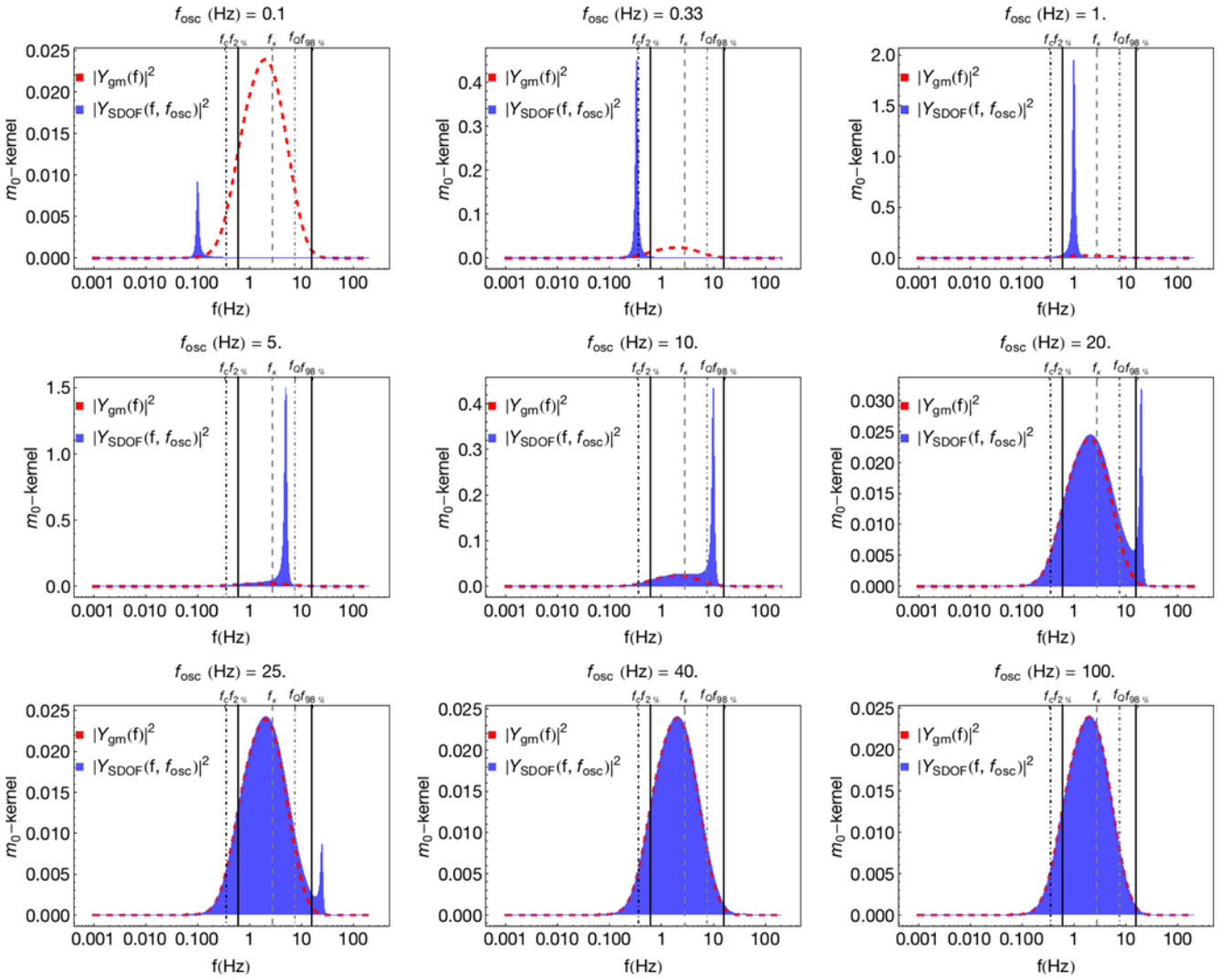

Figure 3. Plots depicting the relative contribution of m_0-kernels $|Y_{SDOF}(f, f_{osc})|^2$ and $|Y_{gm}(f)|^2$ in the square root of the zeroth-spectral moment $m_0(f_{osc})$. The shaded curve indicates the $|Y_{SDOF}(f, f_{osc})|^2$ at different oscillator frequencies f_{osc}. The dashed curve represents $|Y_{gm}(f)|^2$, that is, corresponding to the input ground motion. The plots are shown (with linear vertical axis) for magnitude M_w 6 at a distance $R_{JB} = 20$ km; and the same stochastic model parameters as used for Figure 1. The color version of this figure is available only in the electronic edition.

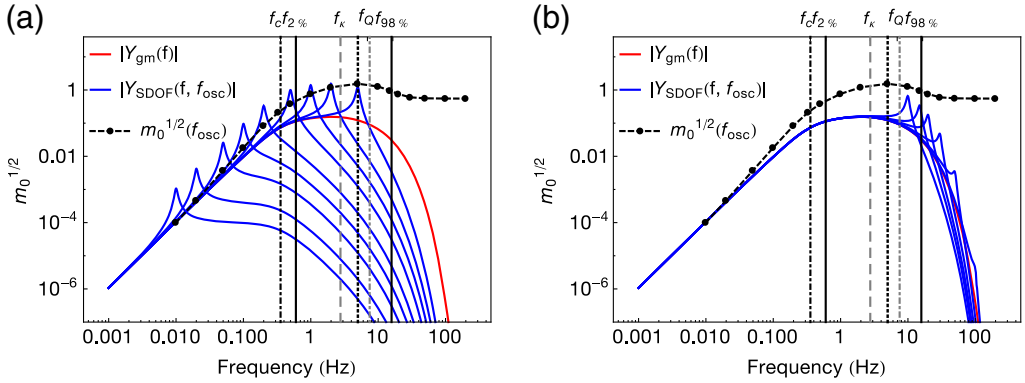

Figure 4. Plots depicting the SDOF oscillator effect $|I(f, f_{osc})|$ at (a) low and (b) high oscillator frequencies, that is, $f_{osc} < f_c$ and $f_{osc} > f_{98\%}$, respectively. The vertical lines correspond to the source-corner frequency, f_c, $f_{2\%}$, half-power points related f_κ and f_Q, and $f_{98\%}$. The dotted vertical line (between f_κ and f_Q) corresponds to the frequency related with the peak of the $y_{max}(f_{osc})$ (5 Hz in this case). The color version of this figure is available only in the electronic edition.

quency the m_0 kernel $|Y_{\mathrm{SDOF}}(f, f_{\mathrm{osc}})|^2$ is dominated by contributions at frequencies well below f_{osc}. Ultimately, for $f_{\mathrm{osc}} > f_{98\%}$ the shape of $|Y_{\mathrm{SDOF}}(f, f_{\mathrm{osc}})|^2$ matches that of $|Y_{\mathrm{gm}}(f)|^2$ making the former a spectrum distributed over a broad range of frequencies similar to the latter. It implies, $m_0^{1/2}(f_{\mathrm{osc}})$ is entirely dominated by $|Y_{\mathrm{gm}}(f)|^2$ regardless of oscillator frequency which consequently makes the $m_0^{1/2}(f_{\mathrm{osc}})$ curve plateau out and to become independent of oscillator frequency (as can also be observed in Fig. 4b).

2. In the middle oscillator-frequency range, that is, $f_{98\%} > f_{\mathrm{osc}} > f_c$ or $f_{2\%}$ (panels in Fig. 3 corresponding to $f_{\mathrm{osc}} = 0.33$–10 Hz), the m_0-kernel function $|Y_{\mathrm{SDOF}}(f, f_{\mathrm{osc}})|^2$ becomes a peaky curve localized at frequencies around f_{osc}; and this peaky part of $|Y_{\mathrm{SDOF}}(f, f_{\mathrm{osc}})|^2$ controls the computation of $m_0^{1/2}(f_{\mathrm{osc}})$ at these oscillator frequencies. Essentially, at f_{osc} below the peak of response spectrum (5 Hz in this example) the $m_0^{1/2}(f_{\mathrm{osc}})$ is determined by a peaky $|Y_{\mathrm{SDOF}}(f, f_{\mathrm{osc}})|^2$ which is mostly localized around the resonance peak of $|I(f, f_{\mathrm{osc}})|^2$ at $f = f_{\mathrm{osc}}$.
3. At low oscillator frequencies (the panel corresponding to $f_{\mathrm{osc}} = 0.1$ Hz) it is again the peaky part of $|Y_{\mathrm{SDOF}}(f, f_{\mathrm{osc}})|^2$ that contributes to the computation of $m_0^{1/2}(f_{\mathrm{osc}})$ at a particular oscillator frequency, but as can be observed from first panel ($f_{\mathrm{osc}} = 0.1$ Hz) in Figure 3 that the shaded $|Y_{\mathrm{SDOF}}(f, f_{\mathrm{osc}})|^2$ curve becomes significantly smaller than the $|Y_{\mathrm{gm}}(f)|^2$ dashed curve. This can be better observed in Figure 4a that $m_0^{1/2}(f_{\mathrm{osc}})$, at $f_{\mathrm{osc}} < f_c$ or $f_{2\%}$, is mainly dominated by the resonant peak of $|I(f, f_{\mathrm{osc}})|$ with some additional contributions from rapidly diminishing amplitudes at $f > f_{\mathrm{osc}}$ as well. However, due to the lower amplitudes of $|Y_{\mathrm{gm}}(f)|$ at those frequencies and clipping-off of high-frequency amplitudes because of the oscillator action, the integration in equation (4) effectively gives a lower $m_0^{1/2}(f_{\mathrm{osc}})$ at those oscillator frequencies.

The higher $m_0^{1/2}(f_{\mathrm{osc}})$ in the oscillator-frequency range $f_{98\%} > f_{\mathrm{osc}} > f_c$ than at $f_{\mathrm{osc}} > f_{98\%}$ indicates that the oscillator action $|I(f, f_{\mathrm{osc}})|^2$ adds extra power to the existing total power (e.g., $m_{0\mathrm{gm}}$) of the input ground motion. Figure 5 depicts the time histories corresponding to the ground-motion $|Y_{\mathrm{gm}}(f)|$ and oscillator response $|Y_{\mathrm{SDOF}}(f, f_{\mathrm{osc}})|$ at different oscillator frequencies. The top-left panel depicts the FAS, $|Y_{\mathrm{gm}}(f)|$, for the earthquake of magnitude M_{w} 6 at a distance $R_{\mathrm{JB}} = 20$ km, the stochastic model parameters remain the same as those used in Figure 1.

The filled circles on the $|Y_{\mathrm{gm}}(f)|$ curve in this panel indicate the oscillator frequencies at which the time series response of the oscillator is computed using the time-domain stochastic simulation method of Boore (2003). The top-right panel in the same figure depicts the response spectra computed using the time-domain simulation, and the predictions obtained from the empirical model of Boore *et al.* (2014) are added to demonstrate the consistency of the simulations. It can be easily observed from the panels (bottom eight) showing the time histories that at $f_{\mathrm{osc}} < f_{2\%}$ (0.6 Hz) the oscillator generates a time history with the lower amplitude indicating a lower power content present in the signal given that the oscillator-response duration is similar to the ground-motion duration. At $f_{\mathrm{osc}} = 2$, 5, and 10 Hz corresponding to the f_{osc} range between $f_{2\%}$ (0.61 Hz) and $f_{98\%}$ (15.8 Hz), it can be observed that oscillator response generates time histories with amplitudes significantly larger than that of the ground motion, this indicates an increase in the signal power due to the oscillator action $|I(f, f_{\mathrm{osc}})|$ on the ground-motion $|Y_{\mathrm{gm}}(f)|$. It can also be observed that at oscillator-frequencies $f_{\mathrm{osc}} \geq 20$ Hz the oscillator response time histories approach the amplitude and shape of input of ground motion which relates to the plateau part of the response spectrum at oscillator frequencies beyond $f_{98\%}$.

The discussion regarding the relationship of FAS and response spectrum in the different oscillator-frequency ranges can be summarized with the help of Figures 6 and 7. In Figures 6 and 7, the simulations are performed for magnitude M_{w} 6 at a distance $R_{\mathrm{JB}} = 20$ km; and the stochastic model parameters remain the same as those used for Figure 1. Figure 6 depicts the contribution of different parts of the m_0 kernel $|Y_{\mathrm{SDOF}}(f, f_{\mathrm{osc}})|^2$ in the computation of $m_0^{1/2}(f_{\mathrm{osc}})$ at a selected oscillator frequency f_{osc}. It was observed in Figure 3 that below the peak of the $m_0(f_{\mathrm{osc}})$ the squared SDOF transfer function amplitude, $|I(f, f_{\mathrm{osc}})|^2$ exerts a strong influence on the computation of $m_0^{1/2}(f_{\mathrm{osc}})$ at a particular f_{osc}. The squared amplitude of SDOF transfer function, $|I(f, f_{\mathrm{osc}})|^2$ that multiplies with $|Y_{\mathrm{gm}}(f)|^2$ to produce $|Y_{\mathrm{SDOF}}(f, f_{\mathrm{osc}})|^2$ can be thought of as being composed of a smooth part and a peaky part that represents the resonance peak of $|I(f, f_{\mathrm{osc}})|^2$. To have a better insight about how each part of $|I(f, f_{\mathrm{osc}})|^2$ influences the computation of $m_0^{1/2}(f_{\mathrm{osc}})$ at a single oscillator frequency f_{osc}, we approximate the smooth part of $|I(f, f_{\mathrm{osc}})|^2$ as $|I(f, f_{\mathrm{osc}}, \zeta = 1/\sqrt{2})|^2$, that is, $|I(f, f_{\mathrm{osc}})|^2$ computed for 70.7% damping as depicted in the Figure 6a. Figure 6b depicts the moment kernels $|Y_{\mathrm{SDOF}}(f, f_{\mathrm{osc}})|^2$ for the two $|I(f, f_{\mathrm{osc}})|^2$ functions (for $\zeta = 0.05$ and $1/\sqrt{2}$) at a selected $f_{\mathrm{osc}} = 15$ Hz. The Figure 6c depicts the $m_0^{1/2}(f_{\mathrm{osc}})$ and $m_0^{1/2}(f_{\mathrm{osc}}, \zeta = 1/\sqrt{2})$ along with the $m_{0\mathrm{gm}}^{1/2}(f_{\mathrm{int}})$ computed from $|Y_{\mathrm{gm}}(f)|^2$. At each f_{osc}, after subtracting the $m_0^{1/2}(f_{\mathrm{osc}}, \zeta = 1/\sqrt{2})$ from $m_0^{1/2}(f_{\mathrm{osc}})$ what remains is the $m_0^{1/2}(f_{\mathrm{osc}})$ contribution that arises from the resonance peak of $|I(f, f_{\mathrm{osc}})|^2$ as represented by the heavy dotted dashed curve in Figure 6c. It can be observed from Figure 6c that $m_0^{1/2}(f_{\mathrm{osc}})$ at high oscillator frequencies, that is, $f_{\mathrm{osc}} > f_{98\%}$ (the plateau) is dominated by the smooth part, which ultimately matches with the $m_{0\mathrm{gm}}^{1/2}(f_{\mathrm{int}})$ and the contribution of resonance peak (heavy dotted dashed curve) de-

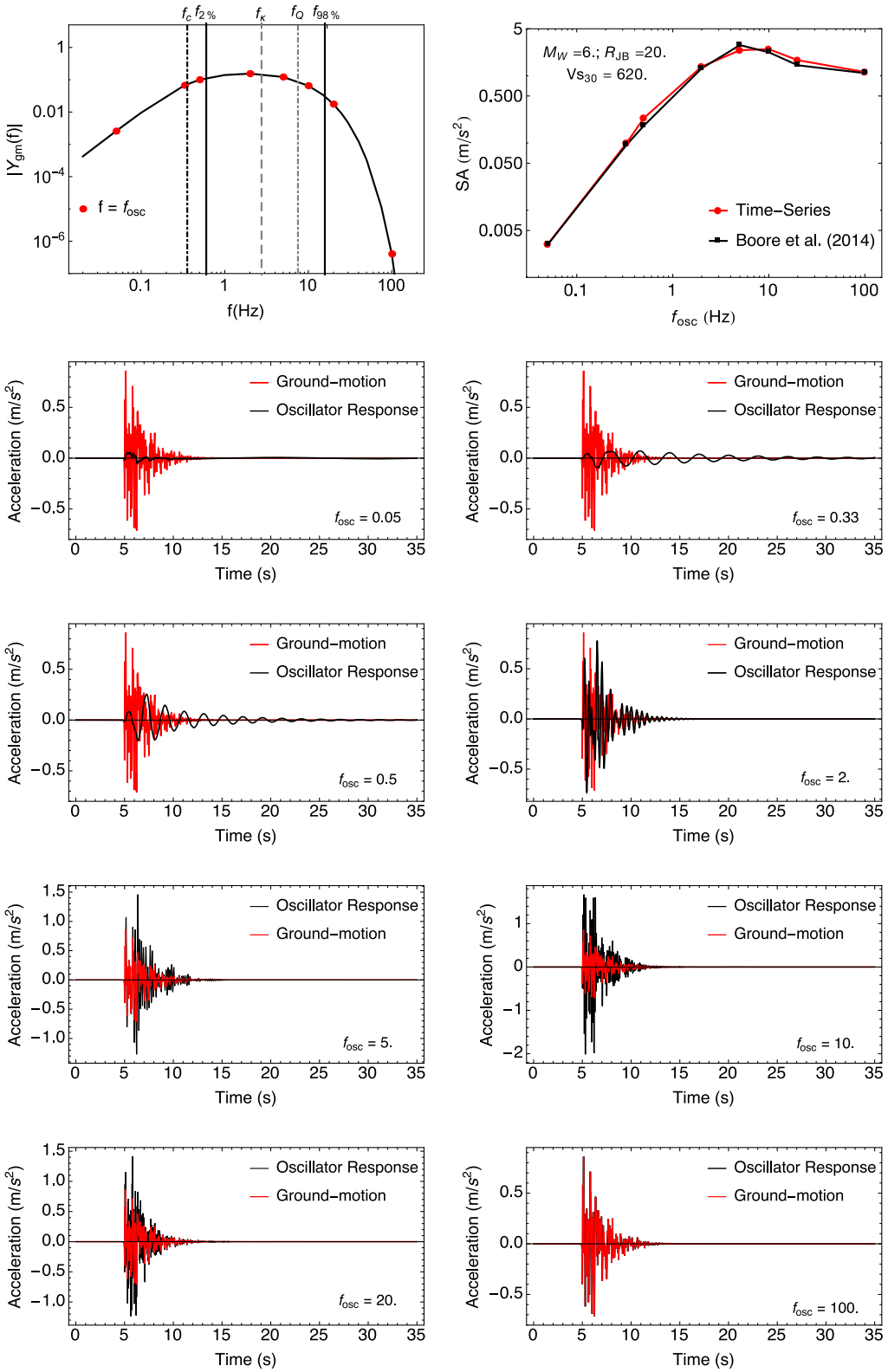

Figure 5. Plots depicting the effect of oscillator response on the input ground motion $|Y_{gm}(f)|$ in terms of the corresponding time histories of oscillator response $|Y_{SDOF}(f, f_{osc})|$. The top-left panel shows the FAS of ground motion, that is, $|Y_{gm}(f)|$, the dark filled circles on the $|Y_{gm}(f)|$ curve indicate the oscillator frequencies at which the time histories for the oscillator response (total acceleration response) are shown in the bottom eight panels. Top-right panel shows the response spectrum obtained from time-series simulation and that from the empirical model of Boore *et al.* (2014). The response spectral ordinates from the time series are computed as the geometric mean over 50 simulations. The color version of this figure is available only in the electronic edition.

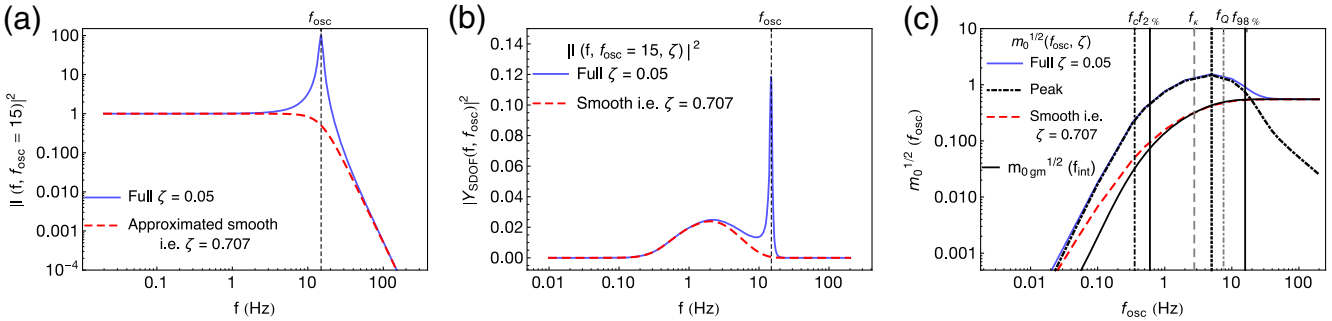

Figure 6. Plots depicting the contribution of smooth and peaky part of the SDOF transfer function (squared amplitude), $|I(f, f_{\text{osc}})|^2$ in the computation of (square root) zeroth-spectral moment $m_0^{1/2}(f_{\text{osc}})$. (a) The full $|I(f, f_{\text{osc}})|^2$ along with the assumed smooth part of it, that is, $|I(f, f_{\text{osc}}, \zeta = 1/\sqrt{2})|^2$. (b) The zeroth-moment (m_0) kernels corresponding to the two transfer functions. (c) The $m_0^{1/2}(f_{\text{osc}}, \zeta)$ for the two transfer functions along with the $m_{0\text{gm}}^{1/2}(f_{\text{int}})$ and the contribution in $m_0^{1/2}(f_{\text{osc}})$ that comes from the peaky part of $|I(f, f_{\text{osc}}, \zeta)|^2$. The contribution of the peaky part (heavy dotted dashed curve) is computed as $m_0^{1/2}(f_{\text{osc}}, \zeta = 0.05) - m_0^{1/2}(f_{\text{osc}}, \zeta = 1/\sqrt{2})$. The color version of this figure is available only in the electronic edition.

creases. As $m_0^{1/2}(f_{\text{osc}}, \zeta = 1/\sqrt{2})$ also matches with $m_{0\text{gm}}^{1/2}(f_{\text{int}})$, this implies that the entire (smooth as well as peak) oscillator action $|I(f, f_{\text{osc}})|^2$ has a minimal effect on the $m_0^{1/2}(f_{\text{osc}})$ and it is the $m_{0\text{gm}}^{1/2}(f_{\text{int}})$ (computed for $|Y_{\text{gm}}(f)|$) that determines the $m_0^{1/2}(f_{\text{osc}})$ at those oscillator frequencies.

However, at low oscillator frequencies, below the peak (dotted vertical line) of the $m_0^{1/2}(f_{\text{osc}})$ the contribution which is coming from the resonance peak of the $|I(f, f_{\text{osc}})|^2$ (heavy dotted dashed curve) matches with the $m_0^{1/2}(f_{\text{osc}})$ indicating that m_0 at these oscillator frequencies is mainly determined by the peaky part of $|I(f, f_{\text{osc}})|^2$. Moreover, using a hypothetical peaky part of $|I(f, f_{\text{osc}})|^2$ Figure 7 illustrates that the contribution of the peaky part of $|I(f, f_{\text{osc}})|^2$ over the entire oscillator-frequency range mimics the shape of FAS implying that below the peak of $m_0^{1/2}(f_{\text{osc}})$, the behavior of the FAS and response spectrum of ground motion with respect to seismological parameters can be considered as equivalent. In Figure 7a, the resonance peak of $|I(f, f_{\text{osc}})|^2$ is approximated by a simple rectangle whose width depends upon the half-power width of the resonance peak. The fractional half-power width ($f_{\text{d}} = 0.057$) of the resonance peak was computed as a fraction of f_{osc} that corresponds to the frequency at which $|I(f, f_{\text{osc}})|^2$ becomes 1/2 times the peak. For the rectangular approximation of the peak, the fractional width of f_{d} was observed to be giving an underestimation of the actual $m_0^{1/2}(f_{\text{osc}})$. Thus, twice of f_{d} was chosen to be the fractional width of the rectangular approximation of the peaky part of $|I(f, f_{\text{osc}})|^2$. Essentially for a selected oscillator frequency, $(1 - 2f_{\text{d}})f_{\text{osc}}$ and $(1 + 2f_{\text{d}})f_{\text{osc}}$ represent the boundaries of the rectangular peak (shown in Fig. 7a) on either side of the corresponding resonant peak of $|I(f, f_{\text{osc}})|^2$. Figure 7b shows the three $|I(f, f_{\text{osc}}, \zeta)|^2$ functions, that is, full, smooth, and approximated, to be used to compute $|Y(f, f_{\text{osc}}, \zeta)|^2$ (in Fig. 7c) and the corresponding $m_0^{1/2}(f_{\text{osc}})$ in Figure 7d. It is worth noting in Figure 7b that the approximated squared amplitude of the transfer function (heavy dashed curve) is obtained as a multiplication of the smooth part (dashed curve) and the rectangular peak (heavy dotted dashed) shown in Figure 7a. The heavy dotted dashed curve in Figure 7d indicates the contribution, of the rectangular peaky part in the approximated $m_0^{1/2}(f_{\text{osc}})$ computed as mentioned in Figure 6. Additionally, $m_{0\text{gm}}^{1/2}(f_{\text{int}})$ is also plotted in the same figure. Similar to our previous observation in Figure 6 it is evident from Figure 7d that at high f_{osc}, the $m_{0\text{gm}}^{1/2}(f_{\text{int}})$ corresponding to the total power in the signal determines the $m_0^{1/2}(f_{\text{osc}})$ at a particular f_{osc}. Below the peak of $m_0^{1/2}(f_{\text{osc}})$, the rectangular peaky part determines the $m_0^{1/2}(f_{\text{osc}})$ and more importantly this heavy dotted dashed curve mimics the shape of the FAS of ground motion. This implies, below the peak of the response spectrum the response spectral scaling can be treated as if they are Fourier spectral ordinates. However, toward higher f_{osc} the full FAS contribution to the determination of a response spectral ordinate is observed. It is worth emphasizing here that Figures 6 and 7 are presented to facilitate a better insight regarding the effect of different parts of $|I(f, f_{\text{osc}})|^2$ that contribute to the computation of $m_0^{1/2}(f_{\text{osc}})$ at a selected f_{osc}. These figures utilize the mathematical approximations for the smooth and peaky part of squared SDOF transfer function $|I(f, f_{\text{osc}})|^2$, and good comparison with the full transfer function enables one to appreciate that these approximations capture the essential features of the problem. However, we are not suggesting that these approximations be used for real applications.

Considering that we have previously shown that the shape of $m_0^{1/2}(f_{\text{osc}})$ is very similar to that of $y_{\max}(f_{\text{osc}})$, the findings regarding the relationship between $m_0^{1/2}(f_{\text{osc}})$ and the FAS of the ground motion $|Y_{\text{gm}}(f)|$ can also be taken to represent the relationship between the Fourier $|Y_{\text{gm}}(f)|$ and response $y_{\max}(f_{\text{osc}})$ spectra. Therefore, this entire discussion implies that the analogy that is often made between the

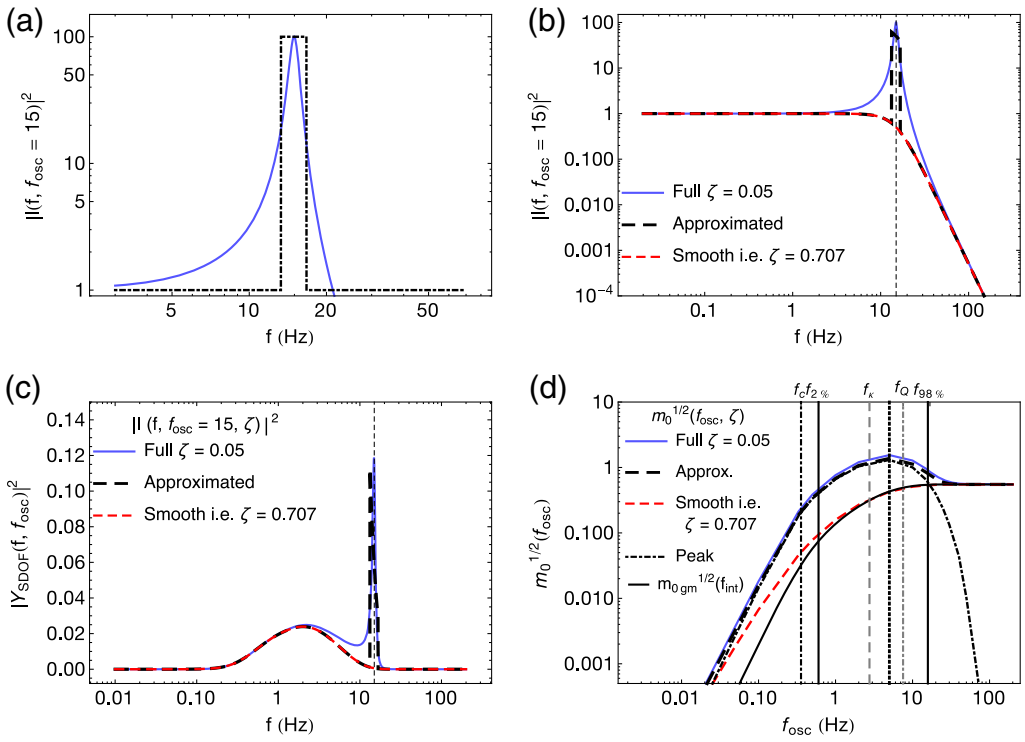

Figure 7. Plots depicting the contribution of smooth and peaky part of the SDOF transfer function (squared amplitude), $|I(f, f_{\text{osc}})|^2$ in which the peaky part of $|I(f, f_{\text{osc}})|^2$ is approximated as a rectangle (a). The width, as a fraction of the oscillator frequency (f_{osc}), of the rectangular peak depends upon the half-power width of the $|I(f, f_{\text{osc}})|^2$. (b) The full $|I(f, f_{\text{osc}})|^2$, smooth part of it, $|I(f, f_{\text{osc}}, \zeta = 1/\sqrt{2})|^2$ and the approximated squared amplitude of the transfer function (heavy dashed curve). (c) The zeroth-moment (m_0) kernels for the three transfer functions. (d) $m_0^{1/2}(f_{\text{osc}}, \zeta)$ for the three transfer functions along with the $m_{0\text{gm}}^{1/2}(f_{\text{int}})$ and the contribution of the rectangular peak (heavy dotted dashed curve). The color version of this figure is available only in the electronic edition.

Fourier and response spectral ordinates is only valid over a limited range of oscillator frequencies. In fact, at high f_{osc} the relationship between the two appears in contrast to the commonly held perception within earthquake engineering that the PGA and other short-period spectral ordinates are high-frequency measures of the ground motion. The analysis just presented using RVT reveals that PGA and other response spectral ordinates at $f_{\text{osc}} > 30$ Hz are related to the entire spectrum of the ground motion. In fact, beyond the highest frequency from which the $|Y_{\text{gm}}(f)|$ decreases the relative contribution of high (Fourier) frequencies decreases with increasing f_{osc}. Essentially, the response spectral ordinate at a selected oscillator frequency depends upon, (1) whether the resonance peak or the smooth part of $|I(f, f_{\text{osc}})|^2$ controls the $m_0^{1/2}(f_{\text{osc}})$ and (2) the position of resonance peak relative to the shape of ground motion FAS, that is, $|Y_{\text{gm}}(f)|$. As can be seen from Figures 6 and 7, at low oscillator frequencies the resonance peak controls the $m_0^{1/2}(f_{\text{osc}})$ whereas at high oscillator frequencies it is the smooth part which controls the $m_0^{1/2}(f_{\text{osc}})$ that ultimately matches with $m_{0\text{gm}}^{1/2}$ at very high oscillator frequencies. The effect of the position of the resonance peak is demonstrated in terms of the location of the oscillator frequency f_{osc} relative to the positions of f_c, f_κ, f_{Q}, or $f_{2\%}$ and $f_{98\%}$. The frequencies are related with the stochastic model parameters $\Delta\sigma$, Q, and κ_0; and these parameters are often used to characterize the shape of the observed FAS. The frequencies $f_{2\%}$ and $f_{98\%}$ can also be thought of as being related to these parameters as they are related with the accumulation of total power contained in the observed FAS. This implies that a change in $\Delta\sigma$, Q, or κ_0 will cause the $y_{\max}(f_{\text{osc}})$ to behave differently at different oscillator frequencies relative to the changed f_c, f_κ, f_{Q}, or $f_{2\%}$ and $f_{98\%}$. Moreover, a change in the shape of $|Y_{\text{gm}}(f)|$ relative to the position of an oscillator frequency f_{osc} will also determine whether the resonance peak or smooth part of $|I(f, f_{\text{osc}})|^2$ controls the $m_0^{1/2}(f_{\text{osc}})$ at that oscillator frequency. That is, the response spectral ordinates will not change in the same way over the entire oscillator-frequency range for a corresponding change in seismological parameters. As mentioned in the Introduction, the ratio of response spectral ordinates (Campbell, 2003) will not necessarily capture the corresponding difference in the FAS of the ground motion. Hence, in what follows we will explore the consequences of the just discussed relationship (similarities and differences) between the FAS $|Y_{\text{gm}}(f)|$ and the response spectrum $y_{\max}(f_{\text{osc}})$ for the adjustment of GMPEs corresponding to changes in the stress parameter $\Delta\sigma$ and the case of site condition adjustment in terms of κ_0 and site amplification. The site-term adjustment in GMPEs has become

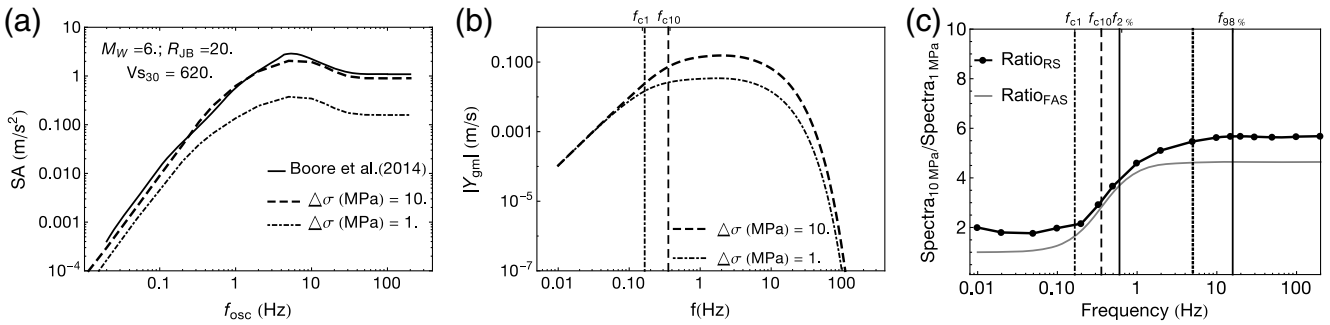

Figure 8. Plots depicting the effect of an adjustment made in the stress parameter $\Delta\sigma$ and its impact on response spectrum, $y_{max}(f_{osc})$ juxtaposed to the FAS, $|Y_{gm}(f)|$ of ground motion. (a) The response spectral ordinates obtained by Boore *et al.* (2014) model along with those obtained by stochastic simulations for $\Delta\sigma$ values 10 (host) and 1(target) MPa. (b) Simulated FAS, $|Y_{gm}(f)|$ for the two $\Delta\sigma$ values. (c) The ratios as $y_{max,10\ MPa}(f_{osc})/y_{max,1\ MPa}(f_{osc})$ and $|Y_{gm,10\ MPa}(f)|/|Y_{gm,1\ MPa}(f)|$ for response spectral ordinates and FAS, respectively. To make the difference more visible between the two ratios, the reciprocal of target amplitudes/host amplitudes is plotted here. The two vertical lines indicate the source-corner frequency $f_{c10} = 0.36$ and $f_{c1} = 0.16$ Hz for $\Delta\sigma = 10$ MPa (dashed) and $\Delta\sigma = 1$ MPa (dotted-dashed), respectively, along with the vertical lines (solid) for $f_{2\%}$ and $f_{98\%}$. The dotted vertical line corresponds to the frequency related with the peak of the $y_{max}(f_{osc})$ (5 Hz in this case).

increasingly important in the context of site-specific seismic-hazard analysis (see e.g., Bommer *et al.*, 2014).

Implications for $\Delta\sigma$ Adjustment

The stress parameter $\Delta\sigma$ is a key parameter in the current practice of ground-motion simulation using the stochastic method as it determines the strength of the high-frequency Fourier spectral amplitude (Atkinson and Beresnev, 1997). Overall, the median value of the $\Delta\sigma$ distribution in a particular region has often been assumed to be constant, though some studies indicate an increase in $\Delta\sigma$ with increasing magnitude, over a limited range of magnitudes typically below **M** 4.5. It is also known that there can be significant regional differences in the value of the median stress parameter. For example, recently Yenier and Atkinson (2015) have found that earthquakes in eastern North America (ENA) attain higher stress parameter values than those in WNA by an average factor of 3. In the context of (median) GMPE adjustment, we investigate the impact of changes in $\Delta\sigma$ on response spectrum, $y_{max}(f_{osc})$ vis-à-vis the FAS of ground motion. This exercise is depicted in Figure 8 in which panel (a) shows the response spectra obtained from the model of Boore *et al.* (2014) and from the stochastic simulations for two values of $\Delta\sigma$. In the context of GMPE adjustment, the values of 10 and 1 MPa could be considered as the host and target values of $\Delta\sigma$, respectively. Therefore, for the present analysis the stochastic model parameters remain the same as those used in Figures 1–3, that is, for WNA (Campbell, 2003) except for the difference in host and target $\Delta\sigma$ values. Figure 8b depicts the FAS of ground motion, that is, $|Y_{gm}(f)|$ corresponding to the two $\Delta\sigma$ values. Figure 8c shows the ratios of FAS and response spectra, for host and target values of $\Delta\sigma$, computed as $|Y_{gm,10\ MPa}(f)|/|Y_{gm,1\ MPa}(f)|$ and $y_{max,10\ MPa}(f, f_{osc})/y_{max,1\ MPa}(f, f_{osc})$, respectively. This plot clearly shows that at $f_{osc} < f_{c1}$ the ratios of stochastically simulated response spectral ordinates are significantly different from the ratios of FAS of the ground motion corresponding to the two values of $\Delta\sigma$. In the frequency range f_{c1}–1 Hz, the two ratios are almost identical. At high oscillator frequencies ($f_{osc} > 1$ Hz) the FAS and response spectral ratios again become significantly different. The differences particularly at high oscillator frequencies cannot be ignored in the adjustment of a GMPE as it can introduce additional epistemic uncertainty through the adjustment process.

The effect of the $\Delta\sigma$ adjustment on the response spectral ordinates can be understood by making use of the similarity between $y_{max}(f_{osc})$ and $m_0^{1/2}(f_{osc})$. This analysis is demonstrated in Figure 9 that depicts the $|Y_{SDOF}(f, f_{osc})|^2$ and the previously defined (see The Building Blocks of Response Spectra section) $m_0(f_{int}, f_{osc})$ computed at different oscillator frequencies f_{osc} corresponding to the two $\Delta\sigma$ values. The plots in Figure 9 are shown for magnitude M_w 6 at a distance $R_{JB} = 20$ km and except for the two different values for $\Delta\sigma$ the stochastic model parameters remain the same as those used in Figure 1.

Figure 9 shows the relative contribution of $|I(f, f_{osc})|^2$ in the computation of $m_0^{1/2}(f_{osc})$ for two host and target stress parameter ($\Delta\sigma$) values 10 and 1 MPa, respectively. In addition to $m_0(f_{osc})$ and $m_{0gm}(f_{int})$ used previously, here we make use of the third measure of m_0, that is, $m_0(f_{int}, f_{osc})$ computed at a particular f_{osc} as a function of f_{int}. The first and third columns in Figure 9 depict $|Y_{SDOF}(f, f_{osc})|^2$ at a particular f_{osc} whereas the second and fourth columns show normalized $m_0(f_{int}, f_{osc})$ at that f_{osc}. The plot of normalized $m_0(f_{int}, f_{osc})$ against frequency f_{int} computed at a particular f_{osc} provides information about the signal frequency range in $|Y_{SDOF}(f, f_{osc})|^2$ that controls the computation of $m_0^{1/2}(f_{osc})$ at that f_{osc}. This frequency range is determined by the use of 2% and 98% limits (in the spectrum) of the final value of $m_0(f_{int}, f_{osc})$ as described in the previous section. The difference between the host and target $m_0^{1/2}(f_{osc})$ becomes evident from the $m_0(f_{int}, f_{osc})$ panel that correspond to $f_{osc} < f_{c1}$,

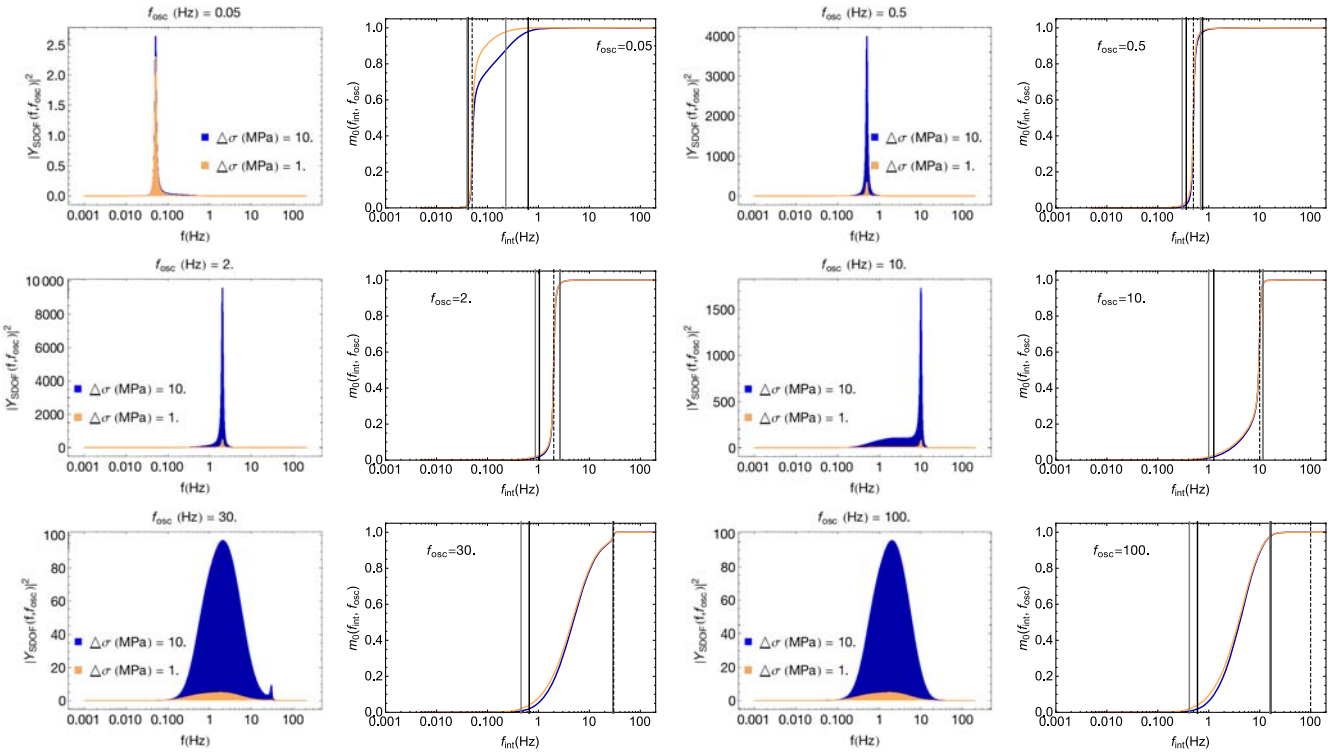

Figure 9. Plots depicting the relative contribution of signal power and oscillator response in the computation of $m_0(f_{osc})$ for two host and target stress parameter ($\Delta\sigma$) values 10 and 1 MPa (in two different shades), respectively. The first and third columns plot the m_0 kernel $|Y_{SDOF}(f, f_{osc})|^2$ at different oscillator frequencies (f_{osc}), whereas the second and fourth column depict normalized $m_0(f_{int}, f_{osc})$ computed at the same f_{osc}. The vertical lines indicate $f_{2\%}$ and $f_{98\%}$ frequencies corresponding to the 2% and 98% values of the final $m_0(f_{int}, f_{osc})$ for the two $\Delta\sigma$ values 10 MPa (dark solid) and 1 MPa (light solid). The dashed vertical line represents the oscillator frequency f_{osc} at which the $m_0^{1/2}(f_{osc})$ is computed. The color version of this figure is available only in the electronic edition.

that is, $f_{osc} = 0.05$ Hz. These plots indicate that the $m_0^{1/2}(f_{osc})$ at $f_{osc} < f_c$ corresponding to 1 MPa is dominated by a relatively short frequency band in comparison (higher frequencies contributing less, note the gray vertical lines) with that corresponding to 10 MPa (dark vertical lines). This makes the ratio of $m_0^{1/2}(f_{osc})$ and therefore of y_{max} at those f_{osc} to be different than that of $|Y_{gm}(f)|$ computed at $f = f_{osc}$. As can be observed from the $m_0(f_{int}, f_{osc})$, plots corresponding to f_{osc} 0.5 and 2 Hz, the $m_0^{1/2}(f_{osc})$ is dominated by almost the same frequency range (for both the values of $\Delta\sigma$) that is mainly coming from the frequencies around the resonance peak f_{osc}. This corresponds to the oscillator-frequency range in Figure 8 where the FAS and response spectral ratios are nearly identical. This smaller mismatch between FAS and response spectral ratios can be better appreciated if the peaky part of $|I(f, f_{osc})|^2$ is regarded as a Dirac delta function $\delta(x)$ and the following property of this function is employed,

$$\int_{-\infty}^{\infty} f(x)\delta(x-a) = f(a). \tag{10}$$

If one relates the functions $f(x)$ and $\delta(x-a)$ from the above equation with $|Y_{gm}(f)|^2$ and $|I(f, f_{osc})|^2$ and variables x and a with f and f_{osc}, respectively, in equations (4) and (5). The $m_0(f_{osc})$ essentially becomes $|Y_{gm}(f_{osc})|^2$ (see equations 4 and 5). The analogy of resonance peak (of $|I(f, f_{osc})|^2$) with $\delta(x)$ is purely mathematical and is only used here to better illustrate the role of the former in computing $m_0(f_{osc})$ at low oscillator frequencies. Nevertheless, this analogy should be considered valid whenever the ratio of two response spectra is identical to that of the corresponding Fourier spectra at a selected oscillator frequency. On the other hand, the significant difference in FAS and response spectral ratios at very low ($f_{osc} < f_{c1}$ in Fig. 8c) and at high oscillator frequencies (see panels corresponding to $f_{osc} = 10$, 30, and 100 Hz in Fig. 9) can be attributed to the differences in the controlling frequency bands (in respective $m_0^{1/2}(f_{osc})$). It can be observed from panels (in Fig. 9) corresponding to $f_{osc} > 1$ Hz the $f_{98\%}$ are identical, but different $f_{2\%}$ limits for the two $m_0(f_{int}, f_{osc})$ indicate that for 1 MPa the contribution from low frequencies is larger in $m_0^{1/2}(f_{osc})$ than for 10 MPa; this difference accounts for the mismatch between the FAS and response spectral ratios at $f_{osc} > 1$ Hz observed in Figure 8. It is also interesting to note that in the panel showing $m_0(f_{int}, f_{osc})$ within Figure 9 corresponding to $f_{osc} = 100$ Hz, the $m_0^{1/2}(f_{osc})$ is mainly controlled by different (wide) bands of frequencies other than the resonance peak (note the

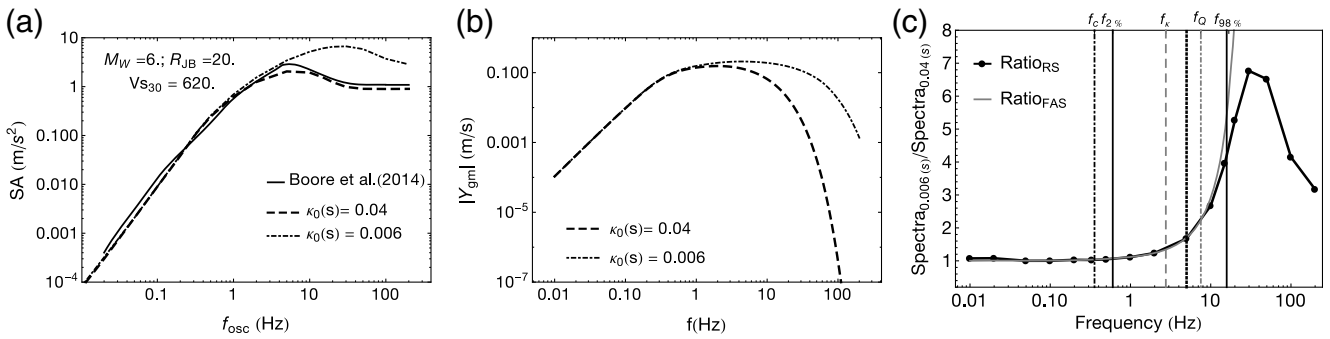

Figure 10. Plots depicting the effect of an adjustment made in the site related attenuation parameter, κ_0 on FAS, $|Y_{gm}(f)|$ and its impact on the response spectrum, $y_{max}(f_{osc})$. (a) The response spectral ordinates obtained from the model of Boore *et al.* (2014) along with those obtained from stochastic simulations for κ_0 values 0.04 (host) and 0.006 (target) (s). (b) Simulated FAS, $|Y_{gm}(f)|$ for the two κ_0 values. (c) The ratios as $y_{max,0.006\ s}(f_{osc})/y_{max,0.04\ s}(f_{osc})$ and $|Y_{gm,0.006\ s}(f)|/|Y_{gm,0.04\ s}(f)|$ for response spectral ordinates and FAS respectively. The vertical lines indicate source-corner frequency f_c (dotted dashed), κ_0 related corner frequency f_κ (dashed gray), and Q related corner frequency f_Q (gray dotted dashed), $f_{2\%}$ and $f_{98\%}$ (solid-black). The dotted vertical line between f_κ and f_Q corresponds to the frequency related with the peak of the $y_{max}(f_{osc})$ (5 Hz in this case).

position of f_{osc}, i.e., dashed vertical line). Essentially, the two ratios will be different whenever the dominating contribution in $m_0(f_{osc})$ will be coming from a band of frequencies because Fourier spectral amplitudes can be different over that frequency band for two different sets of seismological parameters. As can be seen from Figure 8b, in this case the FAS amplitudes are different at frequencies beyond f_{c1}.

Implications for V_S–κ_0 Adjustment

Usually, GMPEs are derived from a database of earthquake records involving recordings from different sites. Therefore, the average deviation of ground motions at a particular site with respect to the predictions from a GMPE is referred to as the site term representing the site-specific site effects. In the context of site-specific PSHA (Bommer *et al.*, 2014; Rodriguez-Marek *et al.*, 2014), the hazard curves corresponding to the reference rock are convolved with the site-response effects and associated uncertainties to generate hazard curves at the final target velocity horizon at which the ground motions are required (Bazzurro and Cornell, 2004). In addition to that, it is also important in site-specific PSHA to account for the deep shear-wave velocity (V_S) structure and the site attenuation parameter (κ_0) related to the site in question. To capture the differences in the V_S structure and κ_0 with respect to a host site, GMPEs are often adjusted to the target site conditions by performing what are referred to as V_S–κ adjustments. Such adjustments are performed using the velocity profiles and κ values (Cotton *et al.*, 2006) for the host and target regions, in which kappa represents the whole path attenuation combining the effects of Q and site kappa κ_0. However, in the current article the discussion will be focused on V_S and κ_0 adjustments, hence it can be regarded as V_S–κ_0 adjustment. As stated in the Introduction, one of the popular frameworks to perform such adjustments is the use of stochastically simulated response spectral ratios suggested by Campbell (2003).

Therefore, in this section we discuss the implications of the just discussed distinctions and similarities between $|Y_{gm}(f)|$ and $y_{max}(f_{osc})$ for V_S–κ_0 adjustments; in which the two components, that is, V_S and κ_0 will be discussed separately. The adjustment related with the difference in κ_0 values is discussed first followed by a V_S profile adjustment. Similar to the analysis presented in the previous section, Figure 10a depicts the response spectral ordinates from Boore *et al.* (2014) and those from RVT simulations corresponding to κ_0 0.04 and 0.006 s representing the host and target values, respectively, in the context of GMPE adjustment. Other than the difference in κ_0 values, the host and target model parameters are assumed to be the same corresponding to the WNA model of Campbell (2003). Figure 10b shows the FAS, that is, $|Y_{gm}(f)|$ of ground motion corresponding to the two κ_0 values. Figure 10c depicts the ratio of FAS, that is, $|Y_{gm,0.006\ s}(f)|/|Y_{gm,0.04\ s}(f)|$ and that of stochastically simulated (using RVT) response spectral ordinates, that is, $|y_{max,0.006\ s}(f_{osc})|/|y_{max,0.04\ s}(f_{osc})|$. The ratios plotted in Figure 10c indicate that the response spectral ratios at oscillator frequencies, $f_{osc} < f_Q$ (7.5 Hz) are able to capture the corresponding relative difference in the FAS; but at $f_{osc} > f_Q$ (of host) the FAS and response spectral ratios are completely different.

Similar to the plots shown in Figure 9, Figure 11 depicts the plots of m_0-kernel function $|Y_{SDOF}(f, f_{osc})|^2$ in the first and third columns whereas the second and fourth column depict the normalized $m_0(f_{int}, f_{osc})$ at different f_{osc}. It can be observed that at f_{osc} below the peak of the $y_{max}(f_{osc})$ which is 5 Hz in this case the $|Y_{SDOF}(f, f_{osc})|^2$ becomes strongly localized around the f_{osc} due to the resonant peak of $|I(f, f_{osc})|^2$ for both the κ_0 values. It can also be noted from the $m_0(f_{int}, f_{osc})$ panels in the top row of Figure 11 that $m_0^{1/2}(f_{osc})$ is mainly contributed to by the same band of frequencies for both κ_0 values and that these are concentrated around the resonance peak of $|I(f, f_{osc})|^2$. As noted

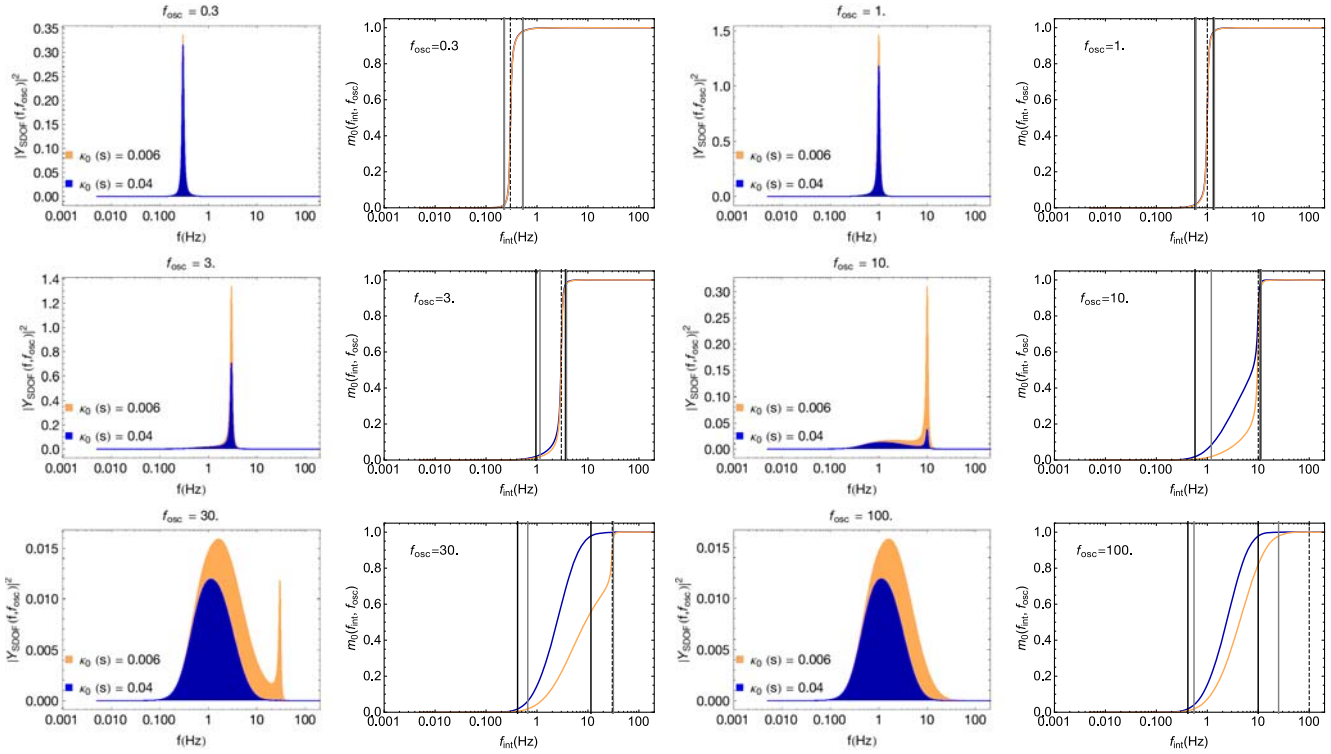

Figure 11. Plots depicting the contribution of signal power and oscillator response in the computation of $m_0(f_{osc})$. The first and third columns depict the m_0-kernel function ($|Y_{SDOF}(f, f_{osc})|^2$) at different oscillator frequencies, f_{osc}, whereas the second and fourth columns depict the normalized $m_0(f_{int}, f_{osc})$ at the same f_{osc}. The two different shades are selected to show these plots for two high-frequency attenuation parameter (κ_0) values 0.04 and 0.006 s, respectively. The vertical lines indicate $f_{2\%}$ and $f_{98\%}$ frequencies corresponding to the 2% and 98% values of the final $m_0(f_{int}, f_{osc})$ for the two κ_0 values 0.04 (s) (dark solid) and 0.006 (s) (light solid). The dashed vertical line represents the oscillator frequency, f_{osc} at which the $m_0^{1/2}(f_{osc})$ is computed. The color version of this figure is available only in the electronic edition.

earlier, the localization of $|Y_{SDOF}(f, f_{osc})|^2$ around a single frequency $f = f_{osc}$ makes the ratios of FAS and response spectral ordinates look identical. At $f_{osc} > f_Q$ (7.5 Hz) a wider spectrum of $|Y_{SDOF}(f, f_{osc})|^2$ takes over in comparison to the localized resonance peak in the computation of $m_0^{1/2}(f_{osc})$. With increasing f_{osc} the width of the significant frequency range, that is, $f_{2\%}$ to $f_{98\%}$ increases differently for the two κ_0 values. For example, at $f_{osc} = 30$ Hz the m_0 corresponding to the host $\kappa_0 = 0.04$ s is dominated by a significantly wider band of frequencies; whereas for $\kappa_0 = 0.006$ s a significant contribution of the resonance peak exists. In effect, at $f_{osc} > f_Q$ (7.5 Hz) the $m_0^{1/2}(f_{osc})$ is dominated by the different frequency ranges corresponding to the two different κ_0 values, as opposed to the case of $f_{osc} < 3$ Hz where the peaky part of $|Y_{SDOF}(f, f_{osc})|^2$ at a single f_{osc} dominates the $m_0^{1/2}(f_{osc})$.

Similar to the cases shown in Figures 8 and 10, Figure 12 depicts the case of V_S profile adjustment, in which Figure 12a shows the response spectral ordinates obtained from the empirical model of Boore *et al.* (2014) along with those obtained from the stochastic (RVT) simulations corresponding to the host and target V_S profiles. Figure 12b shows the FAS of ground motion, that is, $|Y_{gm}(f)|$ corresponding to the two V_S profiles. In the context of GMPE adjustment, we assume that the host profile corresponds to one appropriate for WNA whereas the target profile is representative for ENA. The specific profiles are generically characterized by V_{S30} values of 620 and 2800 m/s, respectively. The amplification corresponding to the two velocity profiles is computed using the quarter-wavelength method (Joyner *et al.*, 1981; Boore and Joyner, 1997). Figure 12c depicts the ratios of FAS and response spectral ordinates computed as $|Y_{gm,2800\ m/s}(f)|/|Y_{gm,620\ m/s}(f)|$ and $|y_{max,2800\ m/s}(f_{osc})|/|y_{max,620\ m/s}(f_{osc})|$, respectively. It can be observed from the ratio plots in Figure 12c that at f_{osc} beyond the peak of the response spectrum (dotted line) the ratio of FAS differs significantly from that of response spectral ordinates.

This difference in ratios can be better explored with the help of Figure 13. Similar to Figures 9 and 11, Figure 13 depicts the m_0-kernel functions $|Y_{SDOF}(f, f_{osc})|^2$ in the first and third columns whereas the second and fouth columns depict the normalized $m_0(f_{int}, f_{osc})$ at a selected f_{osc}. It is evident that at $f_{osc} < 5$ Hz (peak of the response spectrum) the $|Y_{SDOF}(f, f_{osc})|^2$ is concentrated around the resonant peak ($f = f_{osc}$) of the oscillator that dominates the computation of $m_0^{1/2}(f_{osc})$ at the slected f_{osc}. The $m_0(f_{int}, f_{osc})$ pan-

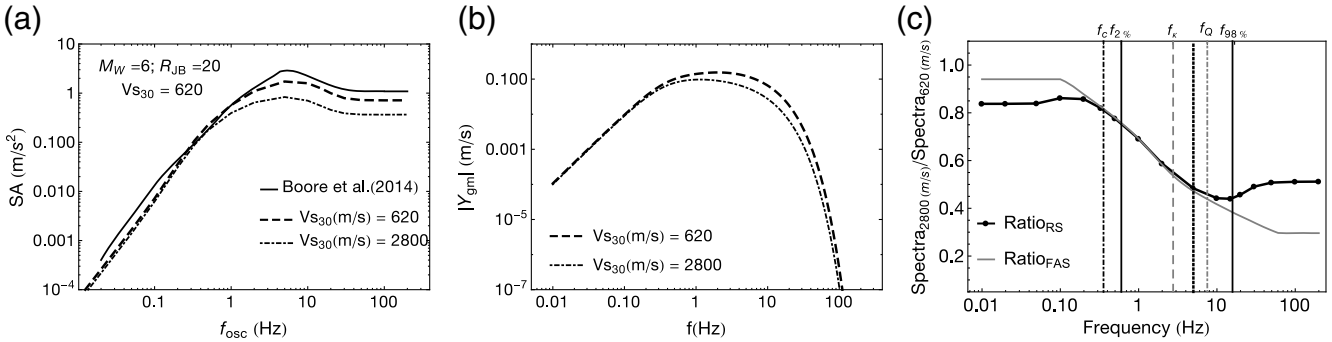

Figure 12. Plots depicting the effect of an adjustment made to the site shear-wave velocity (V_S) profile on FAS, $|Y_{gm}(f)|$ and its impact on the response spectrum, $y_{max}(f_{osc})$ of ground motion. (a) The response spectral ordinates obtained from the empirical model of Boore *et al.* (2014) along with those obtained by stochastic simulations for two V_S profiles corresponding to the average shear-wave velocity in upper 30 m soil column V_{S30} 620 (host) and 2800 (target) m/s. (b) Simulated FAS, $|Y_{gm}(f)|$ for the two V_S profiles. (c) The ratios as $y_{max,2800\ m/s}(f_{osc})/y_{max,620\ m/s}(f_{osc})$ and $|Y_{gm,2800\ m/s}(f)|/|Y_{gm,620\ m/s}(f)|$ for response spectral ordinates and FAS, respectively. The vertical lines indicate source-corner frequency f_c (dotted dashed), κ_0-related corner frequency f_κ (dashed gray), and Q related corner frequency f_Q (gray dotted dashed), $f_{2\%}$ and $f_{98\%}$ (solid black). The dotted vertical line between f_κ and f_Q corresponds to the frequency related with the peak of the $y_{max}(f_{osc})$ (5 Hz in this case).

els ($f_{osc} = 0.3$ and 1 Hz) in the top row of Figure 13 also indicate that the main contribution in $m_0^{1/2}(f_{osc})$ for both the V_S profiles is coming from an identical band of frequencies around the resonance peak (the dashed vertical line). The strong localization of $|Y_{SDOF}(f, f_{osc})|^2$ around f_{osc} makes the ratio of $m_0^{1/2}(f_{osc})$ and hence that of $y_{max}(f_{osc})$ identical to the ratio of $|Y_{gm}(f)|$. As described earlier at oscillator frequencies beyond the peak of the response spectrum the localized behavior of $|Y_{SDOF}(f, f_{osc})|^2$ diminshes and a wideband spectrum overtakes the contribution to $m_0^{1/2}(f_{osc})$ that ultimately matches with $|Y_{gm}(f)|^2$ at a selected f_{osc}, for example, 100 Hz. As can be observed from the $m_0(f_{int}, f_{osc})$ panels corresponding to $f_{osc} > 3$ Hz in Figure 13, two significantly different bands of frequencies are controlling the computation of $m_0^{1/2}(f_{osc})$ at a selected f_{osc} that makes the ratio of $y_{max}(f_{osc})$ in Figure 12 different than the ratio of $|Y_{gm}(f)|$ which is computed at a single frequency $f = f_{osc}$.

Conclusions

The aim of the present article was to provide new insights regarding the distinctions and similarities between the Fourier spectrum and the corresponding response spectrum of ground motion which is observed to have a strong influence regarding the adjustment of response spectral GMPEs to differences in stress and/or site conditions. Often, it has been observed that the concepts from the Fourier spectrum perspective are applied to the corresponding response spectrum of a damped SDOF oscillator without paying much attention to the fact that they essentially represent two different entities. A simple example of this can be found in the functional forms of the response spectral GMPEs which are essentially based upon the scaling laws of Fourier spectral ordinates. In fact, the obscured relationship between FAS and response spectrum of ground motion that is referred to at the developmental stage of a response spectral GMPE can have some undesirable behaviors particularly when they are adjusted to different seismological conditions. For performing host-to-target adjustments of GMPEs, Campbell (2003) proposed a framework that utilizes the ratio of stochastically simulated response spectral ordinates with an inherent assumption that it can capture the relative differences (between host and target) in seismological parameters. As shown in this article, such an assumption can lead to unrealistic ratios, which are essentially not able to capture corresponding relative differences between the Fourier spectra of the host and target regions.

To have better insights regarding the relationship between the FAS and the response spectrum of ground motion, we use RVT, a tool that has been successfully used in the stochastic simulation method by Boore (1983, 2003). Moreover, RVT has also been used within site response analysis to obtain the amplification factors relative to a reference rock spectral acceleration (Rathje and Ozbey, 2006). The stochastic simulation framework of Boore (2003) is used to decipher the relationships between the FAS and the response spectrum of ground motion. Although earthquake records cannot be considered as representing purely stationary signals, the stochastic simulation method has been successfully applied in different parts of the world owing to its simplicity in capturing the basic scaling of high-frequency ground motions with respect to commonly used seismological parameters such as magnitude and distance. That said, the RVT method should be tested and validated in different seismological environments with respect to the observed recordings. Stochastic model parameters appropriate for the WNA region (Campbell, 2003) are used in the present analysis to represent the FAS model for a scenario magnitude of M_w 6 at distance $R_{JB} = 20$ km. The main aspects of this relationship between FAS and response spectrum as deciphered by RVT indicate that the response spectral ordinates at different oscillator frequencies are dominated by different portions of the squared

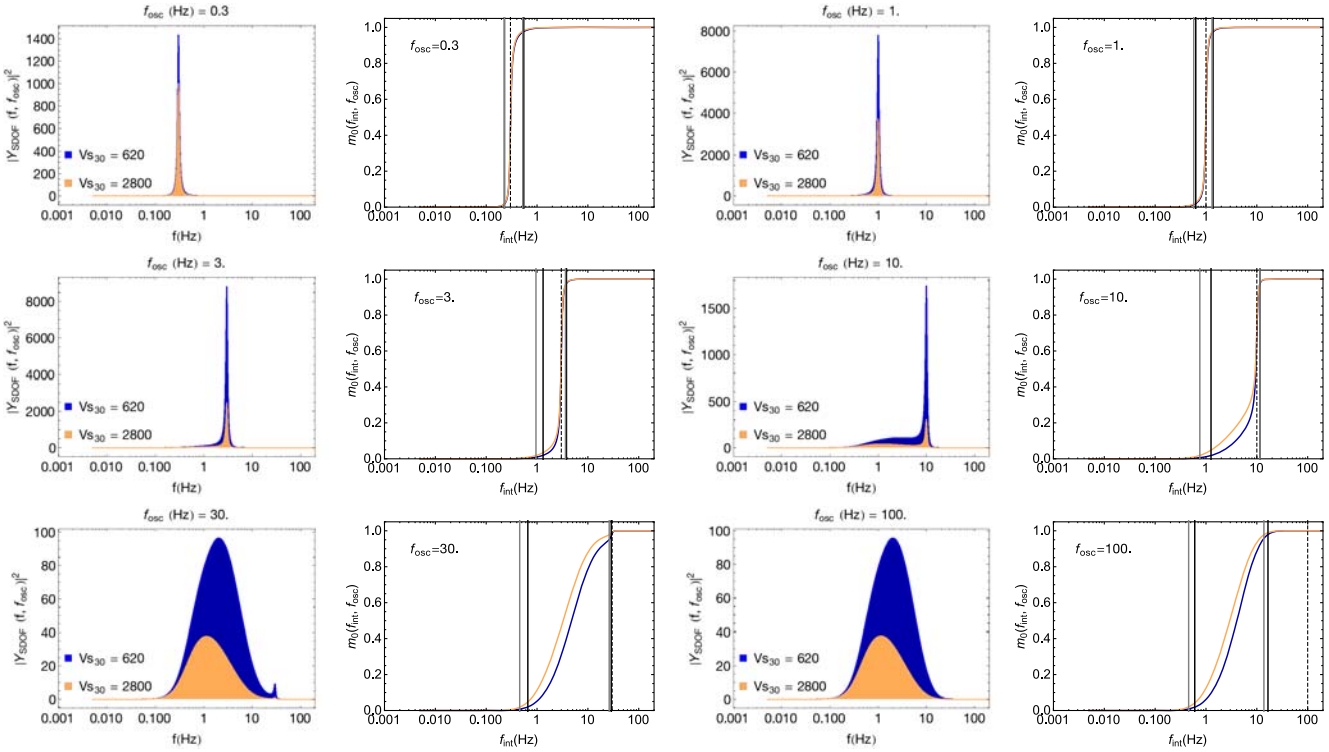

Figure 13. Plots depicting the contribution of signal power and oscillator response in the computation of $m_0(f_{osc})$. The first and third columns depict m_0-kernel function ($|Y_{SDOF}(f, f_{osc})|^2$) at different oscillator frequencies, f_{osc}, whereas the second and fourth columns depict the normalized $m_0(f_{int}, f_{osc})$ at the same f_{osc}. The two different shades are selected to show these plots for two V_S (shear-wave velocity) profiles corresponding to the time-averaged shear-wave velocity in upper 30 m of soil column (V_{S30}) 620 and 2800 m/s, respectively. The vertical lines indicate $f_{2\%}$ and $f_{98\%}$ frequencies corresponding to the 2% and 98% values of the final $m_0(f_{int}, f_{osc})$ for the two V_S profiles related with V_{S30} values 620 m/s (dark solid) and 2800 m/s (light solid). The dashed vertical line represents the oscillator frequency f_{osc} at which the $m_0^{1/2}(f_{osc})$ is computed. The color version of this figure is available only in the electronic edition.

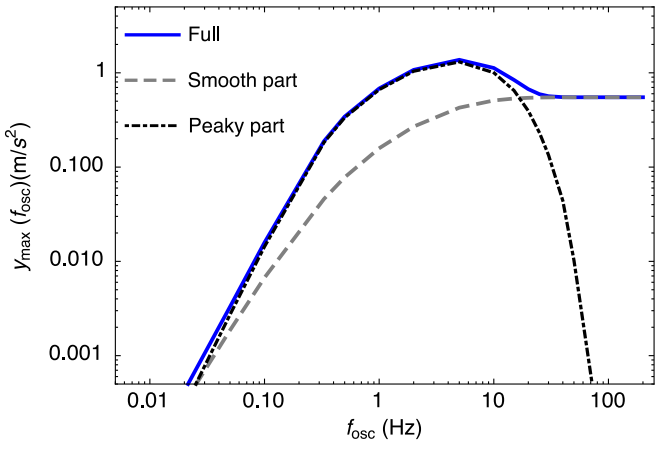

Figure 14. Representation of the response spectrum of an SDOF oscillator (5% damped) excited by the ground-motion acceleration, $|Y_{gm}(f)|$ in terms of the contributions that are coming from the smooth and peaky parts of the SDOF transfer function $|I(f, f_{osc})|$. For having a better understanding about the effect of each part a rectangular peaky part of $|I(f, f_{osc})|^2$ is used for this figure. For more details about the rectangular approximation of the peaky part reader is referred to in Figures 6 and 7. The color version of this figure is available only in the electronic edition.

FAS, that is, $|Y_{gm}(f)|^2$, of ground motion. The entire discussion regarding the relationship of Fourier and response spectra of ground motion can be summarized with the help of Figure 14. It depicts that below the peak of the response spectrum the response spectral ordinates are dominated by the peaky part of oscillator transfer function, $|I(f, f_{osc})|$. Thus, the scaling of response spectral ordinates below the peak of response spectra can be considered equivalent to the scaling of Fourier spectral ordinates at the same frequencies. At high oscillator frequencies (beyond the peak of the response spectrum), the response spectral ordinates are dominated by the smooth part of the oscillator transfer function, a rather wideband spectrum of ground motion that ultimately equals the integration over the entire spectrum of the input ground motion. With respect to PGA (and high-frequency spectral ordinates in general), our RVT-based considerations reveal findings that are contrary to the popular perception that it is assumed to be a high-frequency phenomenon of ground motion. Response spectral ordinates at high oscillator frequencies match asymptotically with PGA but do not correspond to the same frequencies of input ground motion. In fact, PGA and other high oscillator-frequency response spectral ordinates are dominated by the entire frequency-band of ground motion. The counterintuitive behavior of response

spectral ordinates with respect to the FAS of ground motion at high oscillator frequencies can lead to undesirable consequences in the adjustment of response spectral GMPEs. It is shown that for a stress parameter, $\Delta\sigma$ adjustment the response spectral ratios, as suggested in hybrid-empirical approach, do not capture the corresponding ratio of FAS except over a short frequency band at low oscillator frequencies. In the case of site-term (V_S–κ_0) adjustments, at oscillator frequencies below the peak of the host response spectrum, the scaling of response spectral ordinates can be regarded as being equivalent to the FAS of ground motion. Hence, only at those oscillator frequencies the V_S–κ_0 adjustments in GMPEs can be performed by treating the response spectral ordinates on the same footing as the Fourier spectrum of ground motion. An enigmatical behavior of PGA in terms of input FAS requires accounting for the adjustment in the entire FAS of the ground motion.

The entire analysis presented here clearly implies that the response and Fourier spectra cannot be treated in the same way. Moreover, the distinction between the two becomes rather important in the adjustment of a response spectral GMPE. Therefore, any adjustment scheme framed in the response spectral domain may not capture the actual difference that exists between the corresponding Fourier spectra of the host and target regions. The Fourier spectral domain provides a rather physically consistent and transparent way of adjusting the GMPEs in different seismological environments. The GMPE that was first presented in Bora *et al.* (2014) and subsequently improved and updated in Bora *et al.* (2015) can be considered as a beginning in this direction, which essentially combines two separate empirical models for the FAS and duration of ground motion through RVT to obtain the response spectral ordinates. Indeed, the analysis presented in this study provides strong evidence in favor of incorporating physics-based models in seismic-hazard analysis, albeit calibrated with the observed recordings.

Data and Resources

The stochastic model parameters used in this study were considered from table 2 of Campbell (2003). The routines and subroutines for performing simulations were prepared in Mathematica software for performing the entire analysis presented in this study.

Acknowledgments

Sanjay Singh Bora is grateful to the Helmholtz Research School GeoSim for providing a fellowship. This research was partly funded by the SIGMA project. The authors appreciate and thank Fabrice Cotton for feedback provided by him at various stages of the present study. Christian Molkenthin is also thanked for discussion, comments, and feedback, which ultimately led to improvements of the presented analysis. The two reviewers Hiroshi Kawase and Emrah Yenier are also thanked for reviewing the manuscript. The critical comments and feedback provided by both the reviewers have helped improve the manuscript significantly.

References

Arias, A. (1970). A measure of earthquake intensity, in *Seismic Design for Nuclear Power Plants*, R. J. Hansen (Editor), MIT Press, Cambridge, Massachusetts, 438–483.

Atkinson, G. M. (1984). Attenuation of strong ground motion in Canada from a random vibrations approach, *Bull. Seismol. Soc. Am.* **74,** no. 6, 2629–2653.

Atkinson, G. M. (2006). Single-station sigma, *Bull. Seismol. Soc. Am.* **96,** no. 2, 446–455.

Atkinson, G. M., and I. Beresnev (1997). Don't call it stress drop, *Seismol. Res. Lett.* **68,** no. 1, 3–4.

Bazzurro, P., and C. A. Cornell (2004). Nonlinear soil-site effects in probabilistic seismic hazard analysis, *Bull. Seismol. Soc. Am.* **94,** 2110–2123.

Bommer, J. J., K. J. Coppersmith, R. T. Coppersmith, K. L. Hanson, A. Mangongolo, J. Neveling, E. M. Rathje, A. Rodriguez-Marek, F. Scherbaum, R. Shelembe, P. J. Stafford, and F. O. Strasser (2014). A SSHAC level 3 probabilistic seismic hazard analysis for a new-build nuclear site in South Africa, *Earthq. Spectra* **31,** no. 2, 661–698.

Boore, D. M. (1983). Stochastic simulation of high-frequency ground motions based on seismological models of the radiated spectra, *Bull. Seismol. Soc. Am.* **73,** no. 6A, 1865–1894.

Boore, D. M. (2003). Simulation of ground motion using the stochastic method, *Pure Appl. Geophys.* **160,** no. 3, 635–676.

Boore, D. M., and W. B. Joyner (1984). A note on the use of random vibration theory to predict peak amplitudes of transient signals, *Bull. Seismol. Soc. Am.* **74,** no. 5, 2035–2039.

Boore, D. M., and W. B. Joyner (1997). Site amplifications for generic rock sites, *Bull. Seismol. Soc. Am.* **87,** no. 2, 327–341.

Boore, D. M., and E. M. Thompson (2012). Empirical improvements for estimating earthquake response spectra with random-vibration theory, *Bull. Seismol. Soc. Am.* **102,** no. 2, 761–772.

Boore, D. M., J. P. Stewart, E. Seyhan, and G. M. Atkinson (2014). NGA-West2 Equations for Predicting PGA, PGV, and 5% Damped PSA for Shallow Crustal Earthquakes, *Earthq. Spectra* **30,** no. 3, 1057–1085.

Bora, S. S., F. Scherbaum, N. Kuehn, and P. J. Stafford (2014). Fourier spectral- and duration models for the generation of response spectra adjustable to different source-, path- and site conditions, *Bull. Earthq. Eng.* **12,** 467–493.

Bora, S. S., F. Scherbaum, N. Kuehn, P. J. Stafford, and B. Edwards (2015). Development of a response spectral ground-motion prediction equation (GMPE) for seismic hazard analysis from empirical Fourier spectral and duration models, *Bull. Seismol. Soc. Am.* **105,** no. 4, 2192–2218.

Brune, J. (1970). Tectonic stress and the spectra of seismic shear waves from earthquakes, *J. Geophys. Res.* **75,** no. 26, 4997–5009.

Brune, J. (1971). Correction, *J. Geophys. Res.* **76,** no. 20, 5002.

Campbell, K. W. (2003). Prediction of strong ground motion using the hybrid empirical method and its use in the development of ground-motion (attenuation) relations in eastern North America, *Bull. Seismol. Soc. Am.* **93,** no. 3, 1012–1033.

Cartwright, D. E., and M. S. Longuet-Higgins (1956). The statistical distribution of the maxima of a Random function, *Proc. Math. Phys. Sci.* **237,** no. 1209, 212–232.

Cotton, F., F. Scherbaum, J. Bommer, and H. Bungum (2006). Criteria for selecting and adjusting ground-motion models for specific target regions: Application to central Europe and rock sites, *J. Seismol.* **10,** no. 2, 137–156.

Hanks, T. C., and R. K. McGuire (1981). The character of high-frequency strong ground motion, *Bull. Seismol. Soc. Am.* **71,** no. 6, 2071–2095.

Joyner, W. B., R. E. Warrick, and T. E. Fumal (1981). The effect of quaternary alluvium on strong ground motion in the Coyote Lake, California, earthquake of 1979, *Bull. Seismol. Soc. Am.* **71,** no. 4, 1333–1349.

Liu, L., and S. Pezeshk (1999). An improvement on the estimation of pseudoresponse spectral velocity using RVT method, *Bull. Seismol. Soc. Am.* **89,** no. 5, 1384–1389.

McGuire, R. K., and T. C. Hanks (1980). RMS acceleration and spectral amplitudes of strong ground-motion during the San Fernando, California earthquake, *Bull. Seismol. Soc. Am.* **70,** no. 5, 1907–1919.

McGuire, R. K., A. M. Becker, and N. C. Donovan (1984). Spectral estimates of seismic shear waves, *Bull. Seismol. Soc. Am.* **74,** no. 4, 1427–1440.

Rathje, E. M., and M. C. Ozbey (2006). Site-specific validation of random vibration theory based seismic site response analysis, *J. Geotech. Geoenviron. Eng.*, doi: 10.1061/(ASCE)1090-0241(2006)132:7(911).

Rodriguez-Marek, A., E. M. Rathje, J. J. Bommer, F. Scherbaum, and P. J. Stafford (2014). Application of single-station sigma and site-response characterization in a probabilistic seismic-hazard analysis for a new nuclear site, *Bull. Seismol. Soc. Am.* **104,** no. 4, 1601–1619.

Scherbaum, F., J. Schmedes, and F. Cotton (2004). On the conversion of source-to-site distance measures for extended earthquake source models, *Bull. Seismol. Soc. Am.* **94,** no. 3, 1053–1069.

Schneider, J. F., W. J. Silva, S. J. Chiou, and J. C. Stepp (1991). Estimation of ground-motion at close distances using the band-limited white noise model, in *Proceedings, 4th International Conference on Seismic Zonation*, Vol. 4, EERI, Stanford, California, 187–194.

Silva, W. J., N. Abrahamson, G. Toro, and C. Costantino (1997). Description and vliadation of the stochastic ground-motion model, Final report, *Brookhaven National Laboratory, Report Contract No. 770573*, Associated Universoties, Inc., Upton, New York.

Stepp, J. C., W. J. Silva, H. B. Seed, I. M. Idriss, R. McGuire, and J. Schneider (1991). Site response evaluations based upon generic soil profiles using random vibration methodology, *Proceedings, 4th International Conference on Seismic Zonation*, Vol. 4, EERI, Stanford, California, 739–746.

Vanmarcke, E. H., and S.-S. P. Lai (1980). Strong-motion duration and RMS amplitude of earthquake records, *Bull. Seismol. Soc. Am.* **70,** no. 4, 1293–1307.

Yenier, E., and G. M. Atkinson (2015). Regionally adjustable generic ground motion prediction equation based on equivalent point-source simulations: Application to central and eastern North America, *Bull. Seismol. Soc. Am.* **105,** no. 4, 1989–2009.

GFZ, German Research Center for Geosciences
Helomholtzstr. 6
14467 Potsdam, Germany
bora@gfz-potsdam.de
sanjay.singh@geo.uni-potsdam.de
(S.S.B.)

Institute of Earth and Environmental Science
University of Potsdam
Karl-Liebknecht-Str. 24-25
14476, Potsdam, Germany
fs@geo.uni-potsdam.de
(F.S.)

Pacific Earthquake Engineering Research Center
325 Davis Hall
University of California
Berkeley, California 94720-1792
kuehn@berkeley.edu
(N.K.)

Department of Civil and Environmental Engineering
Imperial College London
South Kensington Campus
London SW7 2AZ, United Kingdom
p.sttaford@imperial.ac.uk
(P.S.)

Manuscript received 27 May 2015;
Published Online 24 May 2016